MARIA S. MERIAN-BERICHTE

Morphology, processes and geohazards of giant landslides in and around Agadir Canyon, northwest Africa

Cruise No. MSM32

September 25 – October 30, 2013,
Bremen (Germany) - Cádiz (Spain)

S. Krastel
C. Böttner, M. Cartigny, P. Feldens, L. Fu, S. Glogowski, T. Guggolz, S. Hellmann, V. Hühnerbach, H. Jähmlich, K. Kraus, J. Kretschmer, D. Matthew, D. Meier, I. Mücke, J. von Reumont, M. Schönke, A. Schürer, C. Stevenson, D. Unverricht, D. Voss, A. Webb, R. Wynn

Editorial Assistance:

DFG-Senatskommission für Ozeanographie
MARUM – Zentrum für Marine Umweltwissenschaften der Universität Bremen

2014

The MARIA S. MERIAN-Berichte are published at irregular intervals. They are working papers for people who are occupied with the respective expedition and are intended as reports for the funding institutions. The opinions expressed in the MARIA S. MERIAN-Berichte are only those of the authors.

The MARIA S. MERIAN expeditions are funded by the *Deutsche Forschungsgemeinschaft (DFG)* and the *Bundesministerium für Bildung und Forschung (BMBF)*.

Editor:
DFG-Senatskommission für Ozeanographie
c/o MARUM – Zentrum für Marine Umweltwissenschaften
Universität Bremen
Leobener Strasse
28359 Bremen

Author:
Prof. Dr. Sebastian Krastel
Christian-Albrechts-Universität zu Kiel
Otto-Hahn-Platz 1,
24118 Kiel

Telefon: +49 431 880 3914
Telefax: +49 431 880 4432
e-mail: skrastel@geophysik.uni-kiel.de

Citation: S. Krastel, C. Böttner, M. Cartigny, P. Feldens, L. Fu, S. Glogowski, T. Guggolz, S. Hellmann, V. Hühnerbach, H. Jähmlich, K. Kraus, J. Kretschmer, D. Matthew, D. Meier, I. Mücke, J. von Reumont, M. Schönke, A. Schürer, C. Stevenson, D. Unverricht, D. Voss, A. Webb, R. Wynn (2014) Morphology, processes and geohazards of giant landslides in and around Agadir Canyon, northwest Africa - Cruise MSM32 – September 25 – October 30, 2013 – Bremen (Germany) – Cádiz (Spain). MARIA S. MERIAN-Berichte, MSM32, 53 pp., DFG-Senatskommission für Ozeanographie, DOI:10.2312/cr_msm32

ISSN 2195-8483

Contents

1. Summary

Agadir Canyon is one of the largest submarine canyons in the World, supplying giant submarine sediment gravity flows to the Agadir Basin and the wider Moroccan Turbidite System. While the Moroccan Turbidite System is extremely well investigated, almost no data from the source region, i.e. the Agadir Canyon, are available. Understanding why some submarine landslides remain as coherent blocks of sediment throughout their passage downslope, while others mix and disintegrate almost immediately after initial failure, is a major scientific challenge, which was addressed in the Agadir Canyon source region during Cruise MSM32. We collected ~ 1500 km of seismic 2D-lines in combination with a dense net of hydroacoustic data. About 1000 km^2 of sea floor were imaged during three deployments of TOBI (deep-towed sidescan sonar operated by the National Oceanography Centre Southampton). A total of 186 m of gravity cores and several giant box cores were recovered at more than 50 stations. CTD casts were collected at nine stations including one 13 hour Yo-yo CTD. The new data show that Agadir canyon is the source area of the world's largest submarine sediment flow, which occurred about 60,000 years ago. Up to 160 km^3 of sediment was transported to the deep ocean in a single catastrophic event. For the first time, sediment flows of this scale have been tracked along their entire flow pathway. A major landslide area was identified south of Agadir Canyon. Landslide material enters Agadir canyon in about 2500 m water depth; the material is transported as debrite for at least another 200 km down the canyon. Initial data suggest that the last major slide from this source entered Agadir canyon at least 130,000 years ago. Living deep-water corals were recovered from a large mound field north of Agadir canyon. To our knowledge, these are the first living cold water corals recovered off the coast of Morocco (except for the Gulf of Cadiz). They represent an important link between the known cold-water coral provinces off Mauritania and in the Gulf of Cádiz.

Zusammenfassung

Der Agadir Canyon ist einer der größten Canyons der Welt, durch den große submarine sedimentäre Gravitationsströme in das Agadir Becken und das marokkanische Turbiditsystem transportiert werden. Während das Agadir Becken und das dazugehörige Turbiditsystem sehr gut untersucht sind, existieren fast keine Daten aus dem Agadir Canyon, der das Herkunftsgebiet der großen Turbiditströme darstellt. Die Beantwortung der Frage, warum bei einigen submarinen Hangrutschungen kohärente Blöcke auf ihrer hangabwärts gerichteten Passage bestehen bleiben, während andere Rutschungen sich komplett mischen, ist eine große wissenschaftliche Herausforderung; der Agadir Canyon bietet hervorragende Möglichkeiten, um eine Antwort auf diese Frage zu finden. Während der Fahrt wurde ein dichtes Netz aus hydroakustischen Daten und ca. 1500 km seismischer 2D-Daten aufgezeichnet. Ca. 1000 km^2 Meeresboden wurden im Rahmen von drei TOBI-Einsätzen (tief-geschlepptes Sidescan Sona des National Oceanography Centre Southampton) detailliert abgebildet. Insgesamt wurden 186 Kernmeter mittels Schwerelot und zahlreiche Proben mittels Großkastengreifer gewonnen. CTD-Profile wurden an 9 Stationen aufgezeichnet; darunter war eine Station an der für 13h Profile aufgezeichnet wurden, um einen vollen Tiden-Zyklus zu vermessen. Die neuen Daten zeigen, dass der Agadir Canyon das Herkunftsgebiet der weltweit größten sedimentären Gravitationsströme ist. Bis zu 160 km^3

Sediment wurden während einzelner Ereignisse in die Tiefsee-Becken transportiert. Große Abrisskanten von Rutschungen wurden südlich des Agadir Canyons entdeckt. Das Rutschungsmaterial tritt in ca. 2500 m Wassertiefe in den Canyon ein. Von dort wird das Material noch mindestens 200 km im Canyon als Schuttstrom transportiert. Vorläufige Altersabschätzungen deuten an, dass die letzte große Rutschung aus diesem Gebiet vor ca. 130.000 Jahren stattgefunden hat. Lebende Kaltwasserkorallen wurden in einem großen Hügelfeld nördlich des Agadir Canyons beprobt. Unseres Wissens nach sind dies die ersten Funde lebender Kaltwasserkorallen vor Marokko (mit Ausnahme des Golf von Cádiz). Sie stellen damit ein wichtiges Bindeglied zwischen den bekannten Kaltwasser-Korallen Vorkommen vor Mauretanien und im Golf von Cádiz dar.

2. Participants

Name	Discipline	Institution
Krastel, Sebastian, Prof. Dr. [1]	Chief Scientist	CAU
Schürer, Anke	Seismics	CAU
Böttner, Christof	Seismics	CAU
Hellmann, Sebastian	Seismics	CAU
Fu, Lili	Seismics	CAU
Kretschmer, Jacob	Seismics	CAU
Mücke, Isabell	Seismics	CAU
Jähmlich, Heiko	Tecnician	CAU
Glogowski, Silke	CTD	GEOMAR
Von Reumont, Jonas	CTD	GEOMAR
Unvericht, Daniel	Sedimentology	CAU
Feldens, Peter, Dr.	Sedimentology	CAU
Schönke, Mischa	Sedimentology	CAU
Kraus, Katrin	Sedimentology	CAU
Wynn, Russell, Dr.[1]	Sedimentology	NOCS
Stevenson, Chris, Dr.[1]	Sedimentology	NOCS
Cartigny, Matthieu, Dr.[1]	Sedimentology	UL
Hühnerbach, Veit[1]	TOBI	GEOMAR
Matthews, Duncan[1]	TOBI	NOCS
Webb, Andrew[1]	TOBI	NOCS
Meier, Daniela[2]	Marine Sensor Systems	UO
Voss, Daniela[2]	Marine Sensor Systems	UO
Guggolz, Theresa[2]	Biology	UHH

CAU	Christian-Albrechts-Universität zu Kiel
GEOMAR	Helmholtz-Zentrum für Ozeanforschung Kiel (GEOMAR)
NOCS	National Oceanography Centre Southampton
UHH	University of Hamburg
UL	University of Leeds
UO	Oldenburg University

[1] Only Southampton – Cádiz
[2] Only Bremen –Southampton

3. Research Program

Submarine landslides and sediment gravity flows are the dominant process for sediment transport from the continental shelf to the deep ocean. Sand-rich gravity flow deposits form many of the World's largest oil and gas reservoirs, while mud-rich deposits may sequester globally significant volumes of organic carbon (Galy et al., 2007). Landslides and sediment gravity flows are also a significant geohazard to seafloor infrastructure, e.g. pipelines and telecommunications cables (Camerlenghi et al. 2007; Mosher et al 2010). In some cases, submarine landslides have generated tsunamis that have caused widespread damage to coastal communities (Tappin et al 2001, Bondevik et al 2005).

The largest submarine landslides tend to occur on open areas of the continental slope, in tectonically quiet regions where large volumes of fine-grained sediment can accumulate over long periods of time (Masson et al., 2010). Submarine canyons, such as Agadir canyon may be an important pathway for failed sediments.

Agadir Canyon is one of the largest submarine canyons in the World; it is 450 km long, up to 30 km wide and 1250 m deep. It incises the Morocco Shelf at 200 m water depth and terminates on the floor of Agadir Basin at 4300 m water depth. The upper canyon has two shelf-incising tributaries that merge at a depth of 2200 m; below this the canyon forms a single conduit that curves around a series of seamounts on the lower slope. The Agadir Canyon supplies the World's largest submarine sediment-gravity flows (>100 km^3 volume and up to 2000 km run-out) to Agadir Basin and the wider Moroccan Turbidite System.

The Moroccan Turbidite System has been intensively studied for almost 30 years by NOCS scientists, based upon a dataset comprising over 200 shallow sediment cores. Initial studies were carried out in the deep Madeira Abyssal Plain, which was a proposed dumping site for radioactive waste. Coring and drilling of the plain revealed a long sequence of turbidites, mostly sourced from the Moroccan continental margin and the volcanic Canary Islands. The largest individual flow deposits in the Moroccan Turbidite System contain sediment volumes >100 km^3, although these large-scale events are relatively infrequent with a recurrence interval of ~10,000 years (over the last 200,000 years). The largest siliciclastic flow in the last 200,000 years was the 'Bed 5 event' (Wynn et al., 2010), which transported 160 km^3 of sediment up to 2000 km from Agadir Canyon to the southwest Madeira Abyssal Plain; this run-out distance is exceptional considering that the flow was running across flat (<0.1°) and unchannelised seafloor for more than 50% of that distance. The Bed 5 event occurred at the transition between oxygen isotope stages 4 and 3, at a time when sea level and global temperatures were rising. It therefore seems likely that landslide initiation was linked to rapid sea level rise of ~40 m, following a 10 kyr period of exceptionally low sea level (Siddall et al., 2003).

There are currently very few data from the upper 400 km of this canyon. Hence, the upper part of Agadir Canyon is the missing piece of a jigsaw in order to understand sediment gravity flows from their sources to their final deposits. The upper Agadir Canyon was the main working area of Cruise MSM32 (Figs. 1, 2). Outstanding questions include:

1) What are the location, size and character of the giant landslides scars that represent the source areas of the World's largest sediment-gravity flows? Is there evidence for retrogressive failure? Why do certain landslides transform into turbidity currents and how does this process work?

2) Why does the canyon floor have areas of sandy fill (representing high-energy flows) interspersed with stacked thick (20 m) muddy debris flows, i.e. why do some landslides fully disintegrate while others don't?
3) Why did the devastating 1731 and 1960 Agadir earthquakes not generate a significant landslide or turbidity current in Agadir Canyon?
4) How are huge volumes of material transferred from the Atlas Mountains and Sous River onto the Morocco Shelf and then onwards to upper Agadir Canyon?
5) Can active salt diapirism be identified using onlap relationships of dated debris-flow deposits? How are salt diapirs and debris flows related?
6) Do the large-scale (~500 m wide and ~15 m high) carbonate mounds at ~700 m water depth adjacent to upper Agadir Canyon represent living cold-water coral communities? Cold-water corals are well studied in north-east Atlantic waters, and are a conservation priority.

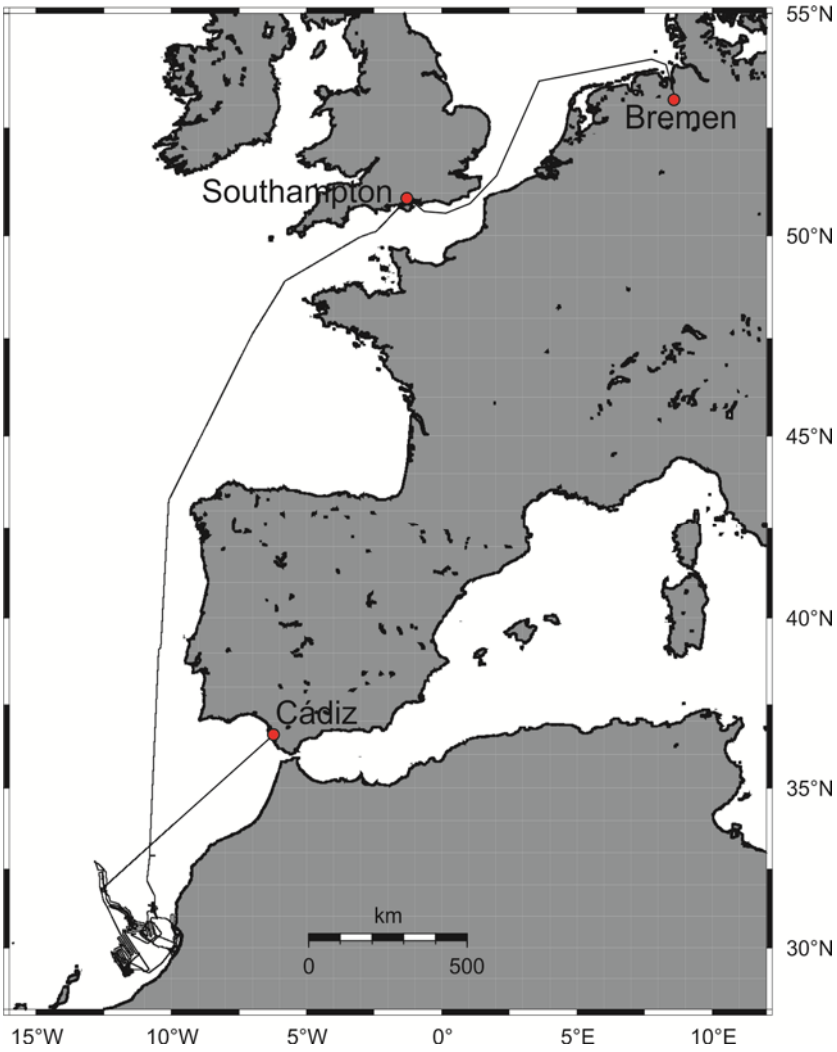

Fig. 1 Cruise track of Cruise MSM32. Details of the working area are shown on Fig. 2.

Methods

The main methods used during Cruise MSM32 are the TOBI deep tow sidescan sonar (operated by the National Oceanography Centre Southampton), a high-resolution 2D seismic system consisting of a 150 m-long 88 channel digital streamer and a standard 1.7 l GI-Gun, geological sampling with gravity corer and giant box corer, CTD measurements as well as the hydroacoustic systems of RV MARIA S. MERIAN.

We originally worked in four main working areas. The focus of a working area south of Agadir Canyon was the investigation of the location, size, and character of giant landslide scars and deposits (Area 1). Work along the canyon axis investigated sediment transport processes through the canyon and possible flow transformations (Area 2). Mass wasting and cold-water carbonate mounds were studied north of Agadir canyon (Area 3). Work on the shelf focussed on sediment transfer from the Atlas Mountains and Sous River onto the Morocco Shelf and then onwards to upper Agadir Canyon (Area 4).

Only minor problems occurred during the cruise. We had some delays due to a water leakage in the TOBI system at the beginning of the cruise. Hence, the amount of collected TOBI-data is less than proposed but we used this additional time for widespread hydroacoustic mapping of this fascinating part of the NW-Atlantic-Continental margin. A very valuable data- and sample set of sediment cores in combination with seismic, sidescan sonar (TOBI) and hydroacoustic data will allow investigating the morphology, processes and associated geohazards of giant landslides in and around Agadir Canyon.

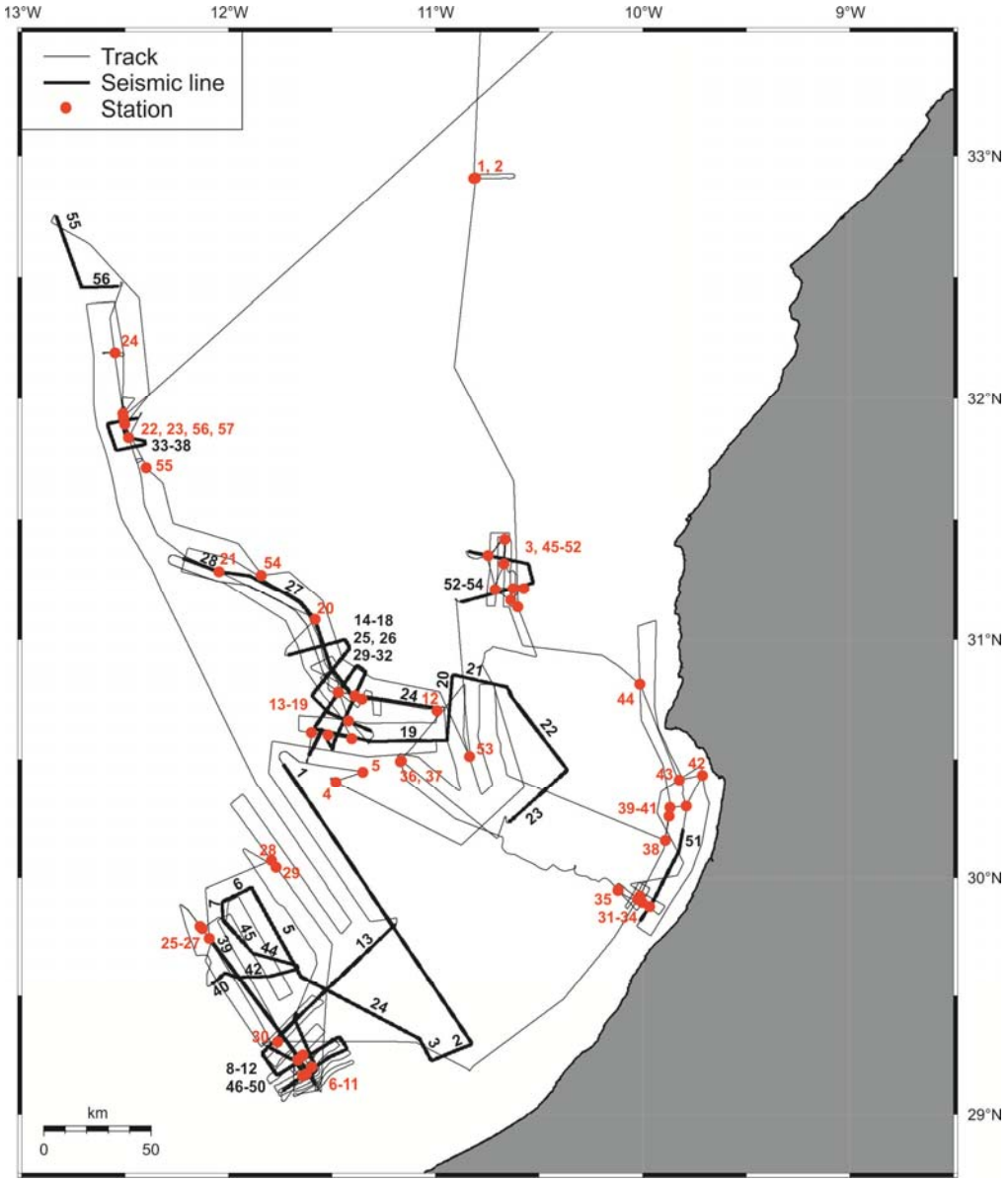

Fig. 2 Track plot of the working area. Red number correspond to geological stations. Black number show line number of seismic profiles.

4. Narrative of the Cruise

The majority of the scientific party arrived in Bremen on September 24th and directly boarded RV MARIA S. MERIAN. Containers were unloaded and MERIAN left the port of Bremen heading to Southampton on September 25th at 08:00h local time. RV MARIA S. MERIAN arrived in Southampton at the pier of the National Oceanography Centre (NOCS) on September 27th at 08:30h. The main aim of this short port call was to load the deep-towed sidescan sonar TOBI and to embark additional scientists.

Loading activities were finished early afternoon and RV MARIA S. MERIAN left the port of Southampton on September 27th at 16:00h. The scientific crew included 11 scientists from the Christian-Albrechts-Universität zu Kiel, 3 scientist from the Helmholtz Centre for Ocean Research Kiel (GEOMAR), 5 scientists from the National Oceanography Centre in Southampton (NOCS) and 1 scientist from Leeds University. Weather during the transit to the Moroccan margin was reasonable with some scattered showers but calm sea state. September 30th was used for short successful test deployments of the TOBI vehicle and the seismic streamer. We entered Moroccan waters around 09:00h on October 1st, which was the start of the scientific program by switching on the hydroacoustic systems. We reached our first station at the distal El Hadiba Canyon early afternoon the same day. A CTD (Station MSM32-1) down to 4200 m was taken for measuring a sound velocity profile for the multibeam systems. Two short hydroacoustic profiles were recorded in order to define potential locations of distal turbidites in the Seine abyssal plane. The PARASOUND showed a promising location (Station MSM32-2) but heavily consolidated sediments resulted in a bended core barrel. The night was used for a transit to an area north of Agadir canyon, where old sediment echo sounder data indicated the presence of carbonate mounds. The new multibeam data clearly show abundant mounds in water depths between ~650 m and 850 m. This area was selected for a first full TOBI deployment on October 2nd at 09:30h. The TOBI data show clear variations in backscatter between individual mounds suggesting that some mounds are active while others are partly covered by sediments. Based on these results, we selected one mound for taking a giant box corer (Station MSM32-3). The box corer sampled both dead and living *Lophelia pertuba* and was therefore a full success. Water samples and a CTD profile were taken at the location of the box corer. The night was used for hydroacoustic surveying of the Agadir Canyon head region. We reached Station MSM32-4 south of Agadir Canyon at 06:00h on October 3rd. This station was targeting landslide deposits identified on available hydroacoustic data. We recovered a giant box corer and a 7.70 m-long sediment core from this location. The core does not show typical landslide deposits suggesting that landslide deposits are covered by a significant drape or that blocks with an intact internal structure were cored. The next station (MSM32-5) was supposed to be in background sediments but sediment recovery was only ~3 m. In the following, we collected two long seismic profiles reaching from ~3000 m depth to the shelf break. These profiles show abundant near surface and buried mass transport deposits. Smaller landslides originate at the flanks of widespread diapirs. The seismic and hydroacoustic also indicate one main fairway for sediment transport into the Agadir Canyon. We started a systematic hydroacoustic survey on October 5th in order to identify the source area of the fairway. We crossed the headwall area for the first time in the morning of October 6th. Individual scarps are up to 100 m high; the complex pattern suggest a multiple stage failure and close interaction of landslide and canyon processes. The data were used to locate three gravity cores (MSM32-06 – 08) in order to sample landslide deposits and the potential glide plane.

Especially Core MSM32-08 shows nice debrite deposits and a potential glide plane in about 7 m subsurface depth. The following night was used for additional hydroacoustic surveying of the headwall area. A TOBI deployment covering the headwall area was scheduled for the morning of October 7th. The CTD mounted on TOBI, however, failed and TOBI was recovered again. A software failure was identified as most likely problem and after fixing this bug, TOBI was deployed again in the afternoon. The same behavior was observed and additional instruments failed. TOBI was recovered again and a small leak in one of the pressure bottles was identified as reason for the cascading-type of failure. As parts of the electronics and the pressure bottle needed severe maintenance, we continued the hydroacoustic mapping during the night. Three successful up to 5 m long gravity cores (MSM32-09 - 11) were taken the next morning (07.10). The aim was to sample different levels of potential glide planes. All cores except for one show clear indications for sediment transport features and potential glide planes. Coring was followed by a seismic survey of the headwall area. The seismic data image a complex interplay between diapirism, canyon processes and mass wasting. As TOBI repairs were still ongoing, we decided to leave the headwall area in order to map the main mass transport fairway entering the deep Agadir Canyon. This attempt was interrupted by a successful test of the damaged pressure TOBI bottle. The new hydroacoustic data allowed to locate three coring locations (MSM32-13 – 15) targeting undisturbed background sediments and different landslide facies; up to 8 m-long gravity were recovered at the these locations on October 10th. The first core was taken in the axis of a small channel in the fairway and shows clear landslide deposits at its base. The second core shows the same deposits overlain by a ~30 cm thick turbidite. The third core was a reference core outside the landslide deposits.

Coring was followed by the next TOBI-deployment in the afternoon of October 10th. All instruments worked fine but the noise level increased significantly with dive depth indicating another malfunctioning. TOBI was brought back on deck and a partly broken cable in the umbilical was quickly identified as reason for the high noise level. As several hours were needed to replace the cable, seismic profiles across Agadir Canyon were collected in the night. The data show that the main transport fairway for landslides to Agadir canyon has been active for a long period of time. Reflection seismic profiling was continued until the morning of October 12th. The umbilical was replaced in the meantime and TOBI deployment started after lunch. This time TOBI worked without any problems and we collected two adjacent profiles (down and upslope) of the thalweg of Agadir Canyon. The TOBI-data show a sandy thalweg and widespread debrite deposits of varying fabric. Numerous slides are entering the canyon from the canyon flanks. TOBI operations had to be stopped on October 14th in the evening due to strong winds form the NE (Beaufort 7-8). The night was used to collect hydroacoustic profiles across Agadir Canyon. The next day (15.10) was an intense and very successful coring day. We started with a boxer core and a gravity core of the sandy thalweg; we recovered thick turbidites and coarse gravel at the base of the gravity core (Station MSM32-16). The following stations aimed in coring debrite deposits, which entered the canyon from the fairway (MSM32-16 to 19). All cores recovered the debrite; the drape on top of the debrite is much thinner in Agadir Canyon compared to the fairway. The debrite shows clear signs of erosion at its top. Seismic profiles across the canyon were collected during the night. October 16th was used to collect a set of cores down the Agadir Canyon (MSM32-20 - 22) in order to investigate the behavior of the debrite when moving downslope inside the canyon. Surprisingly the debrite shows a very consistent appearance down

to ~31°53'N, 12°30'W where hydroacoustic data image a change of the acoustic facies. The final core was taken in the evening of October 16th (MSM32-22) at this location. This core bounced but we recovered a ~2 m long intact section showing a brownish drape overlying a debrite with almost vertically aligned clasts. This may be the edge of a freezing debrite. The night was used for additional seismic imaging of the debrite in the lower Agadir Canyon. Two more cores were taken until early afternoon on October 17th. The first core (MSM32-23) shows very clear signs of flow transformation. The second core (MSM32-24) was taken further downslope and brought no recovery indicating a hard sandy canyon floor at this location.

We left the lower Agadir Canyon around 16:00h on October 17th and started a transit to the headwall area mapped earlier in order to collect TOBI data of this region. TOBI and the airgun seismics were successfully deployed in the evening of October 18th at very calm seas. The seismic data show an interesting step like pattern in the headwall region. The TOBI data show relative homogeneous low-back scatter data as the slide deposits are covered by a thick hemipelagic drape. TOBI was recovered after one long downslope-run in the evening of October 19th. Additional seismic data across the mass transport deposits were collected in the night. The seismic data show a clear relationship between slide thickness and flow behavior on one side and diapirs on the other hand. Slide material moved around the diapirs and left only thin deposits on their tops. October 20th was a successful coring day. We started with three cores (MSM32-25 – 27) about 40 km downslope of the main headwall across the boundary of a debrite. These cores show a very interesting transition from debritic deposits over slightly deformed deposits to undisturbed deposits outside the slide. Afterwards two additional cores were taken in the depositional part of the debrite (MSM32–28, 29). Additional seismic data across the headwall area were collected during the night. The data indicate that sediment waves play an important role in controlling the locations of individual failures. A last core (MSM32-30) targeting the glide plane of the slide was successfully taken in the morning of October 21st. Afterwards we started a hydroacoustic survey of the shelf around the the Sous river mouth and the head region of Agadir Canyon. Surprisingly no indications for incised valleys were identified in the data. Several features indicate that the sediment freight of the Sous River is transported to the north though the shelf region around Agadir Canyon itself is presently sediment starved. A tributary canyon approximately 100 km south of the head region of Agadir Canyon cuts into the shelf. Several box cores were taken in the head region of this tributary canyon; fine sand is the dominant material in this area. A core in the thalweg of this canyon in ~800 m water depth shows about 80 cm hemipelagic sediment on top of an immature turbidite. The night was used for mapping the tributary canyon; the course of the canyon is strongly controlled by diapirs. Two cores were taken late evening on October 23rd. A giant box corer was taken from the thalweg of the tributary canyon about ~120 km off the shelf break while a gravity core targeted a terrace in direct vicinity. The terrace is about 90 m higher than the thalweg. Core recovery was a bit more than one meter because the sandy base of a turbidite prevented further penetration of the gravity corer. This shows that turbidity currents were large enough for depositing significant sand layers about 90 m above the thalweg. October 24th was used for additional coring on the shelf. Different facies were samples by the giant box corer and gravity corer. Fine sand is the dominant sediment on the shelf but a small mud belt was identified off Agadir in a mid-shelf position.

After finishing the shelf work in the late evening of October 24th, we headed to the coral area identified at the beginning of the cruise. Additional mapping showed that an area of about 400

km^2 between 650 m and 850 m water depth is covered with abundant mounds. We sampled six of these mounds distributed across the entire area and in different water depth by means of the giant box corer (Stations MSM32-45 - 50). Dead *lophelia pertusa* and some other species were found in all box cores. Living corals were found in two box cores in the southern part of the mound field. One of these stations was chosen for a 13-hour yo-yo CTD covering a full tidal cycle (MSM32-51). CTD profiles of all other box corer stations and one additional background station (MSM32-52) were collected on October 26th in order to investigate differences in the oceanographic setting between living and dead coral sites. The coral work was completed by two seismic profiles crossing different parts of the field. October 27th was used to collect additional cores of Agadir Canyon. The first core (MSM32-53) was taken high above the canyon thalweg in order to check whether major turbidity currents occurred in the upper Agadir Canyon in the past. The core contains only one single turbidite with coarse pebbles at its base suggesting that it was a very energetic and large flow, possibly representing Bed 5 identified in the Moroccan turbidite system. Three additional cores (MSM32-54 – 56) taken on October 27th; these cores recovered different debris flow facies from distal Agadir Canyon. The research program was completed by a small seismic survey of distal Agadir Canyon and one final core (MSM32-57). We started our transit to Cádiz at 21:30h on October 28th; we arrived at the port of Cádiz as scheduled on October 30th at 08:30h.

RV MARIA S. MERIAN-Cruise MSM32 was a great success. We collected about 1500 km of seismic 2D-lines in exceptional quality. We had three successful TOBI deployments covering an area of about 1000 km^2. We collected about 186 m of cores at 40 stations. In addition, we took 22 giant box cores. CTD casts were collected at 9 stations including one 13 hour Yo-yo CTD. Hydroacoustic data were collected during designated surveys as well as along all seismic profiles and transits. The new data will allow an in depth investigation of the morphology, processes and geohazards of giant landslides in and around Agadir Canyon.

5. Preliminary Results

5.1. Hydroacoustics

5.1.1. Bathymetric mapping

(P. Feldens, C. Böttner, S. Hellmann, L. Fu, , J. Kretschmer, I. Mücke, A. Schürer)

Technical description

During Cruise MSM32, the hull-mounted Kongsberg Simrad systems EM122 and EM1002 were used for bathymetric mapping. The deep water system EM122 was operated continuously in a 24-hour schedule. Several surveys were especially designed for collecting multibeam data. The shallow water system EM 1002 was only used during a shelf survey.

The EM122 system allows an accurate bathymetric mapping down to full ocean depth. Basic components of the system are two linear transducer arrays in a Mills cross configuration with separate units for transmitting and receiving. The nominal sonar frequency is 12 kHz with an angular coverage sector of up to 150° and 864 soundings per ping. In typical ocean depths, a sounding spacing of about 50 m across and along is achievable. The achievable swath width on a flat bottom will normally be up to six times the water depth. The angular coverage sector and beam pointing angles may be set to vary automatically with depth according to achievable coverage. This maximizes the number of usable beams. The beam spacing is normally

equidistant, but an equiangular mode is also available. Using the detected two-way-travel-time and the beam angle known for each beam, and taking into account the ray bending due to refraction in the water column due to sound speed variations, depths are calculated for each beam. A combination of amplitude (for the central beams) and phase (slant beams) is used to provide a measurement accuracy practically independent of the beam pointing angle. Beside the depth values, the EM122 provides also backscatter information and pseudo-sidescan images.

The EM 1002 multibeam echo sounder is a very high-resolution seabed mapping system for shallow waters. The EM 1002 transducer array is used to both transmit and receive. It has a semicircular design with a radius of 45 cm, which was deployed in the starboard moon pool. The EM1002 operates effectively at a variety of depths including shallow coastal waters. The minimum acquisition depth is from 2 m below its transducers, and the maximum acquisition depth is specified down to 1000 m. During the cruise, we used the system only for water depth less than ~400. Across-track coverage is approximately 1500 meters in deep water and up to 7.4 times the depth in shallow water. Normal angular coverage is adjustable up to 150°. During the cruise, the swath width was adjusted manually to get the best compromise between coverage and data quality with changing water depth and sea state. The EM 1002 operates at sonar frequencies of 95 kHz. The hydroacoustical transmission fan is divided into three separate sectors when the angular coverage is larger than approximately 100°. To avoid problems associated with multiple echoes due to normal incidence, specific frequencies are used for the inner and outer fan sectors, respectively. Each of these sectors are transmitted sequentially within a single ping. Three different pulse lengths are available, 0.2, 0.7 and 2 milliseconds. Longer pulse lengths usually perform best at depths greater than 600 meters and shorter pulse lengths at depths less than 200 meters. The beam width of the system is 2 x 2 degree. The maximum ping rate is > 10 Hz. The number of beams per ping is 111. The beam spacing may be set to equiangular or equidistant, the latter used during MSM32. A combination of phase and amplitude bottom detection algorithms is used in order to provide soundings with the best possible accuracy. Additionally, an integrated seabed acoustical imaging capability is included as standard.

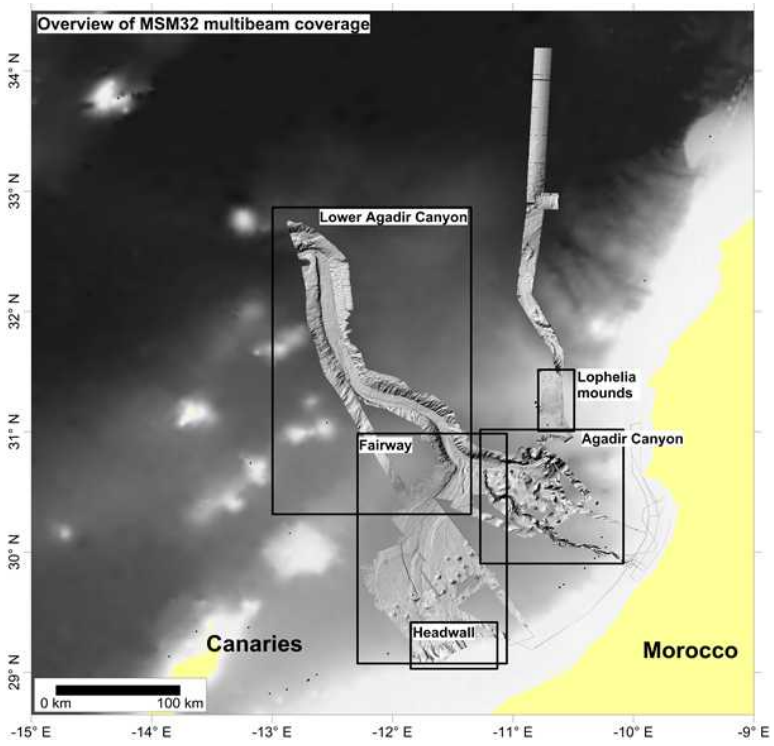

Fig 3 Overview image of all bathymetric data collected during MSM32. The locations of Figs. 4-7 are indicated. Bathymetry shown in the background originates from the GEBCO dataset.

All data were quickly processed

using QPS FLEDERMAUS and MBSYSTEM software. Preliminary processing included general quality checks (navigation, attitude data, sound velocity profiles), the generation of a CUBE surface, and the removal of spikes especially at the overlapping parts of the individual profiles. Further, backscatter images were produced using the QPS GEOCODER software. All grids and images created during this cruise are in stored in geographic coordinates with the WGS84 ellipsoid. All data were imported in the Global Mapper software. A map of all available bathymetric data collected during MSM32 and detailed images of different morphological features are shown on Figs. 3 - 7.

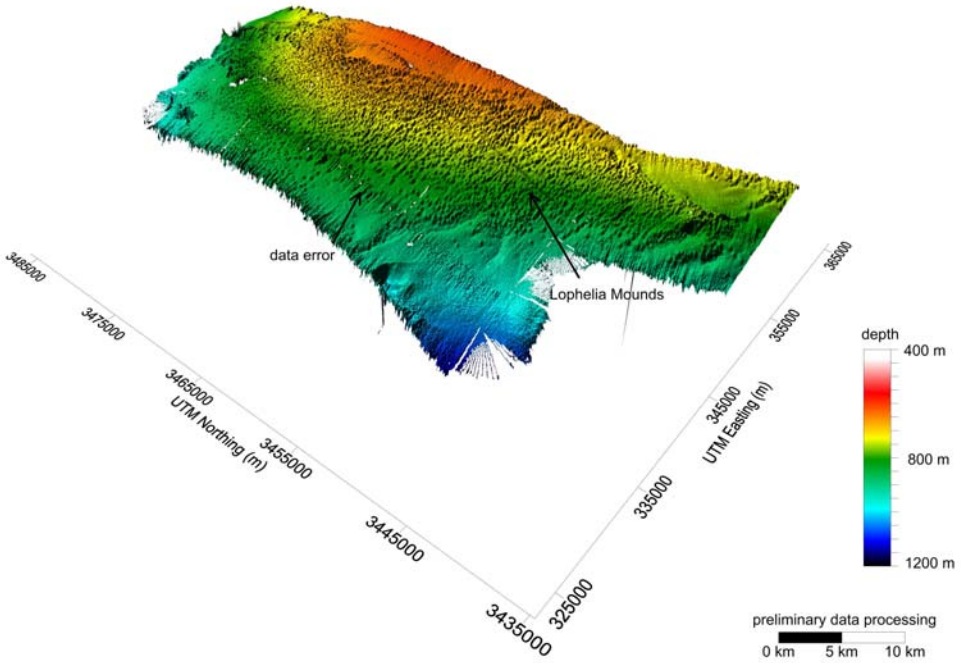

Fig 4 Bathymetric map of the area covered by *Lophelia* mounds. Coral mounds are found in depths between approx. 650 m and 850 m fringing the south-western wall of a local elevation. See Fig. 3 for location.

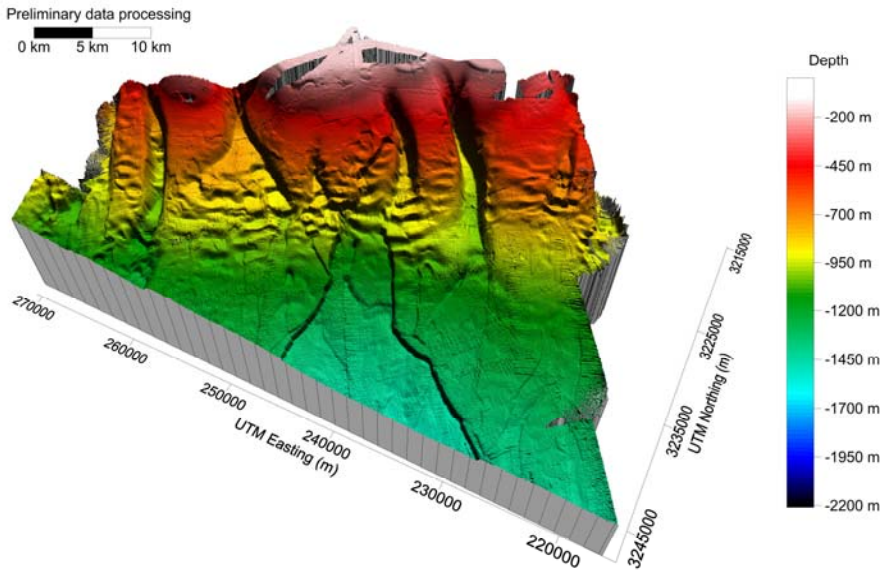

Fig 5 3D Surface of the headwall area of the main debris flow pathway surveyed during MSM32. Next to the headwall area of the flow itself, a series of sediment waves parallel to the depth isolines are observed. See Fig. 3 for location.

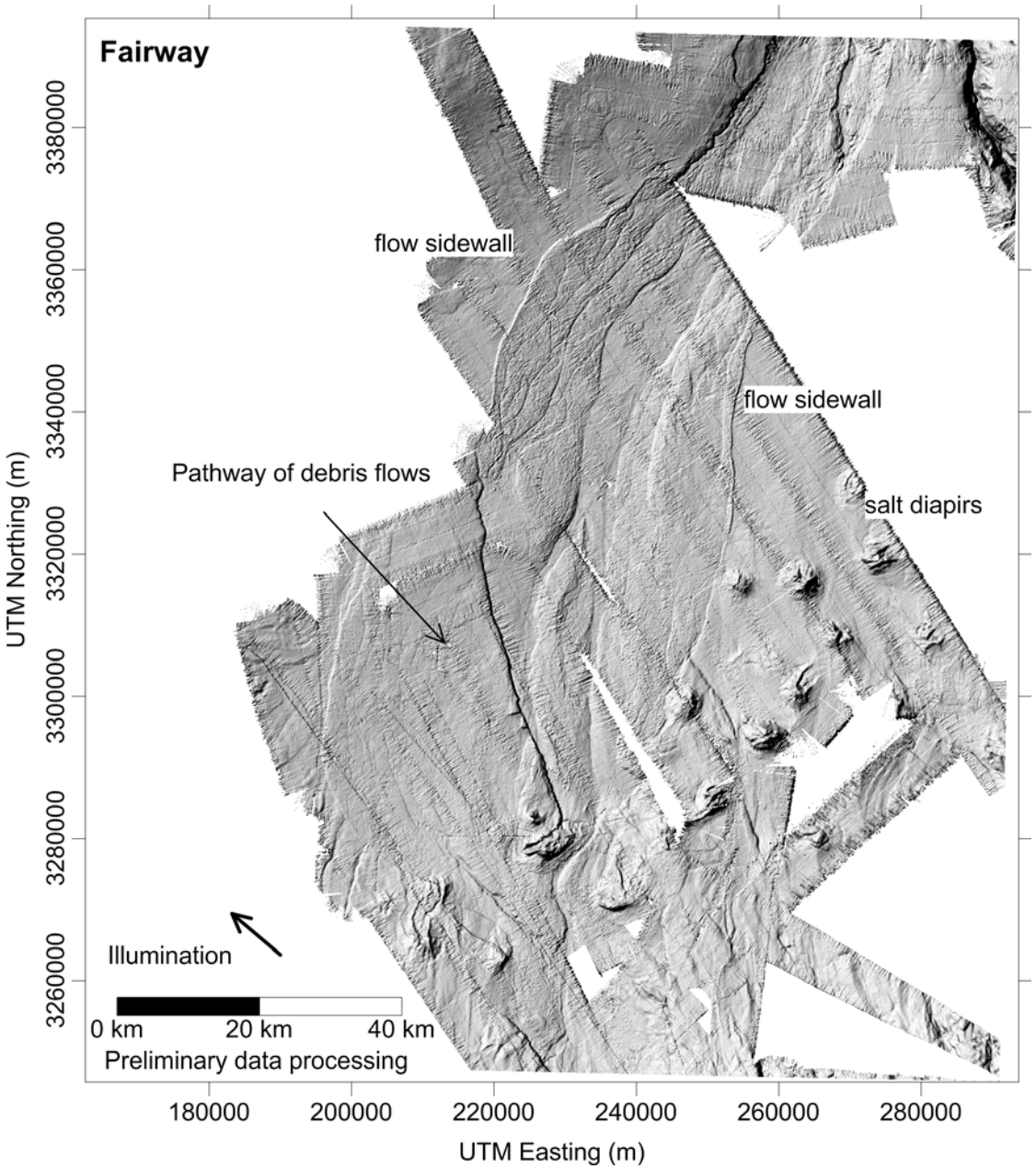

Fig 6 Main pathway of debris flows in the working area as observed in a shaded relief image. Several stages of debrite flowage are indicated by the different sidewalls. The locations of failure are likely controlled by numerous salt diapirs. See Fig. 3 for location.

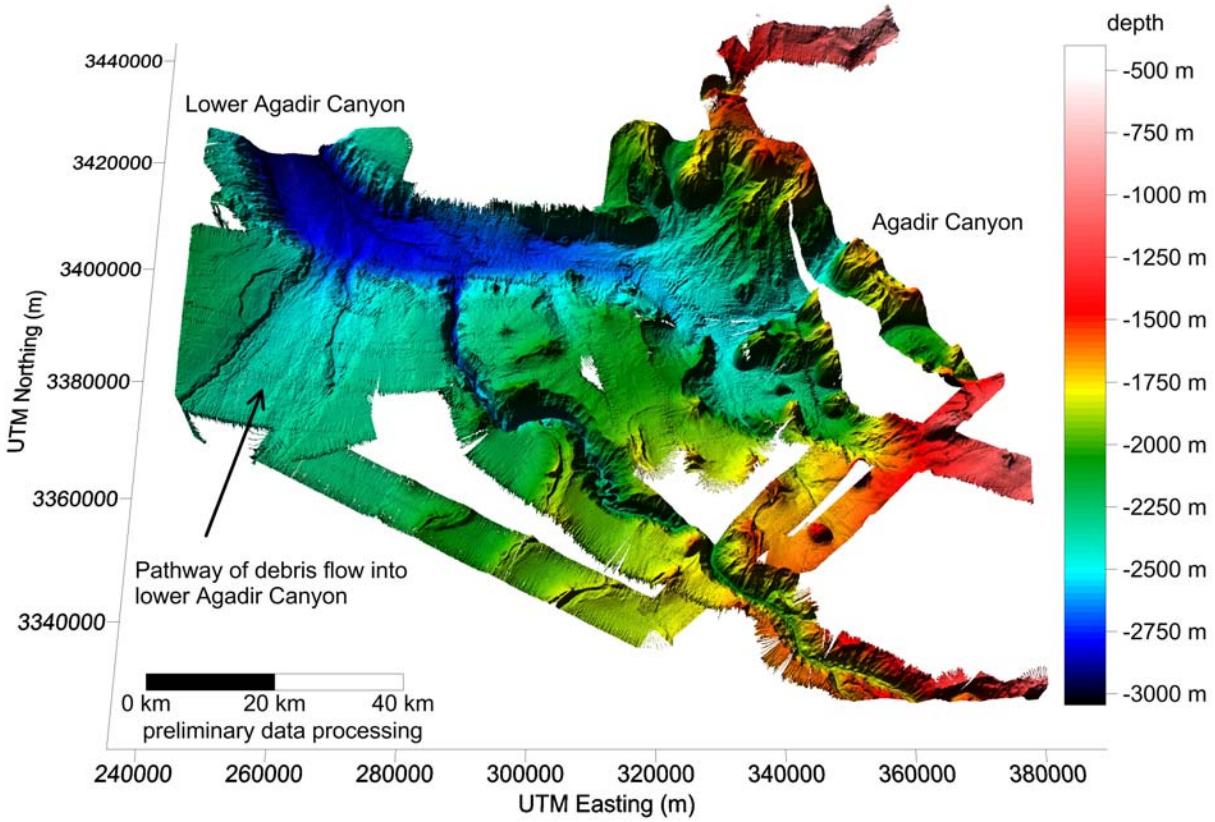

Fig. 7 Newly recorded data from the eastern Agadir Canyon. Remarkable features are debris flow deposits originating from the headwall area shown in Fig. 5 that could be traced into the Lower Agadir Canyon. The morphological onset of the tributary merging with the main Agadir Canyon from the south-east could be located on the mid-shelf in approx. 200 m water depth. See Fig. 3 for location.

5.1.2. Sediment echo sounding

(C. Böttner, L. Fu, , S. Hellmann, J. Kretschmer, I. Mücke, A. Schürer)

System description

The Atlas Parasound system P70 uses the parametric effect, which occurs when very high (finite) amplitude sound waves are generated. If two waves of similar frequencies are generated simultaneously, also the sum and the difference of the two primary frequencies are emitted. For the Parasound System, 18 kHz is one fixed primary frequency, which is generated by a transducer of ~ 1m length within a beam of 4.5°. The second primary frequency can be varied between 18.5 and 24 kHz, resulting in difference frequencies from 0.5 to 6.0 kHz. This signal travels within the 18 kHz beam, which is much narrower than e.g. a 4 kHz signal, emitted from the same transducer directly (30°). Therefore, a higher lateral resolution can be achieved, and imaging of small-scale structures on the sea floor is superior to conventional systems. As another consequence, the signal bandwidth is also increased, and much shorter signals can be generated with improved vertical resolution. Due to the narrow beam, it is necessary to control beam direction, to compensate the ship's movement, and to send the energy vertically downwards. The system treats three signals separately: the primary high frequency signal (18 kHz; PHF), the secondary low frequency signal (selectable 0.5 to 6.0 kHz; SLF) and the secondary high

frequency (selectable 36.5 to 42 kHz; SHF). We selected 4 kHz as SLF and 40 kHz as SHF but only recorded the SLF and PHF signals.

The Parasound system uses minimum different computer systems. Two of them control real-time signal generation and data acquisition through a Linux and a Windows system. The third PC is available for the operator. This Operator-PC hosts the Hydromap Database Server, the Hydromap Control Software and the ParaStore 3 Software. The Hydromap Control Software is responsible for all system settings and for communication with the real-time computers. The ParaStore Software Package is used for visualization, online processing, and data storage. Data can be stored in the Parasound ASD format, but also in the more common PS3 or SEG-Y formats. Several windows can be opened to display different signals (PHF, SLF, SHF) with different scaling and/or processing parameters. This allows optimizing the windows for specific purposes, as e.g. imaging of the upper 20 m of sediments to select optimal coring locations, to choose a full penetration plot, which also allows coverage of the topography, or to study the complete water column.

The system can be used in the single pulse mode, when a single pulse is emitted and the water column and sediment response are recorded before the next pulse is sent, or in the pulse train or quasi-equidistant mode, by which the two-way travel time of the signal in the water column is used to emit additional signals. Depending on water depth, the signal density can be increased by as much as a factor of 16.

We operated the system mainly in the quasi-equidistant mode, which worked very well during the cruise. Raw ASD data were collected for both the PHF and SLF signal. In addition, we recorded PS3 data of the PHF signals over a time window between 200 m and 300 m and PS3 and SGY-data over the same time window for the SLF-frequency. The PHF depth was used as system depth for most of the time.

System crashes were significantly less infrequent than during previous cruises. Occasionally, communication between the different computers was lost and could be only established by a hard reset of all components. Data gaps, however, are relatively small.

PS3 data for the SLF data were converted to SGY-data covering one profile or 1h – 2h using the software ps32sgy (Hanno Kiel, Bremen University). This data were then loaded to IHS Kingdom for immediate analysis of the data especially in order to select coring locations.

Preliminary results:

Parasound data were recorded along all seismic profiles and on all transits. A few examples are shown in the following.

Fig. 8 shows a Parasound-profile crossing the southern sidewall of a major landslide south of Agadir Canyon about 10 km downslope of the main headwall. The sidewall has a height of almost 100 m. The background sediments south of the sidewall are imaged as well stratified undisturbed sediments but a transparent unit close to the sea floor indicates redeposited sediments. These sediments are clearly cut by the sidewall. The slide shows a clear erosive pattern close to the headwall. Only a thin transparent unit represents the mass transport deposits, which seem to be covered by an undisturbed drape. The deposits clearly thin out to the sidewall. The aim of station MSM32-30 close to the sidewall was to penetrate through the glide plane of the slide, which was well achieved with a gravity core; the glide plane can easily be identified in 110 cm core depth.

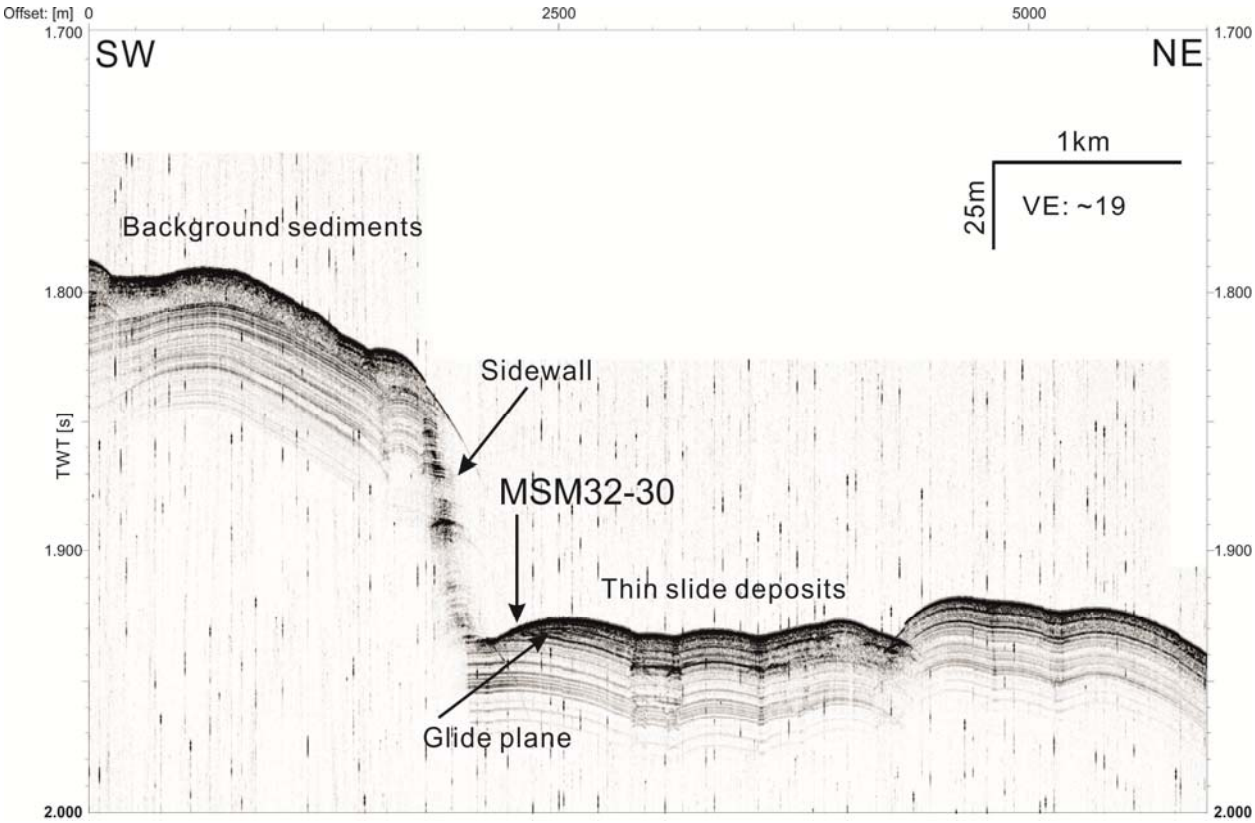

Fig. 8 Parasound profile crossing a sidewall of a major mass wasting event south of Agadir Canyon. Core MSM32-30 aimed in penetrating through the glide plane of the landslide. Location of profile is shown on Fig. 19.

Fig. 9 shows a profile crossing the main pathway of slides south of the Agadir Canyon. Undisturbed deposits are imaged west and east of the so-called fairway, which is the main sediment transport pathway into the Agadir Canyon. The western margin of the fairway shows a ~75 m-high pronounced sidewall indicating that the slide is still mainly erosive in this part. Slide deposits of a secondary failure with a ~20 m-high headwall are imaged west of the main sidewall. The deposits west of the secondary headwall show a few small offset faults, which may represent incipient failures. They may have developed due to the missing support of the sediment mobilized in the debris flow and possibly mark the location of future failures. The eastern margin of the main fairway is characterized by a depositional boundary. Block debris overtop the surrounding background sediments. The fairway itself shows blocky debrite deposits though roughness varies across the fairway. An almost 40 m-deep channel cuts the debrite deposits. The channel is partly filled with acoustic transparent units. Cores MSM32-13 to 15 were taken along this profile.

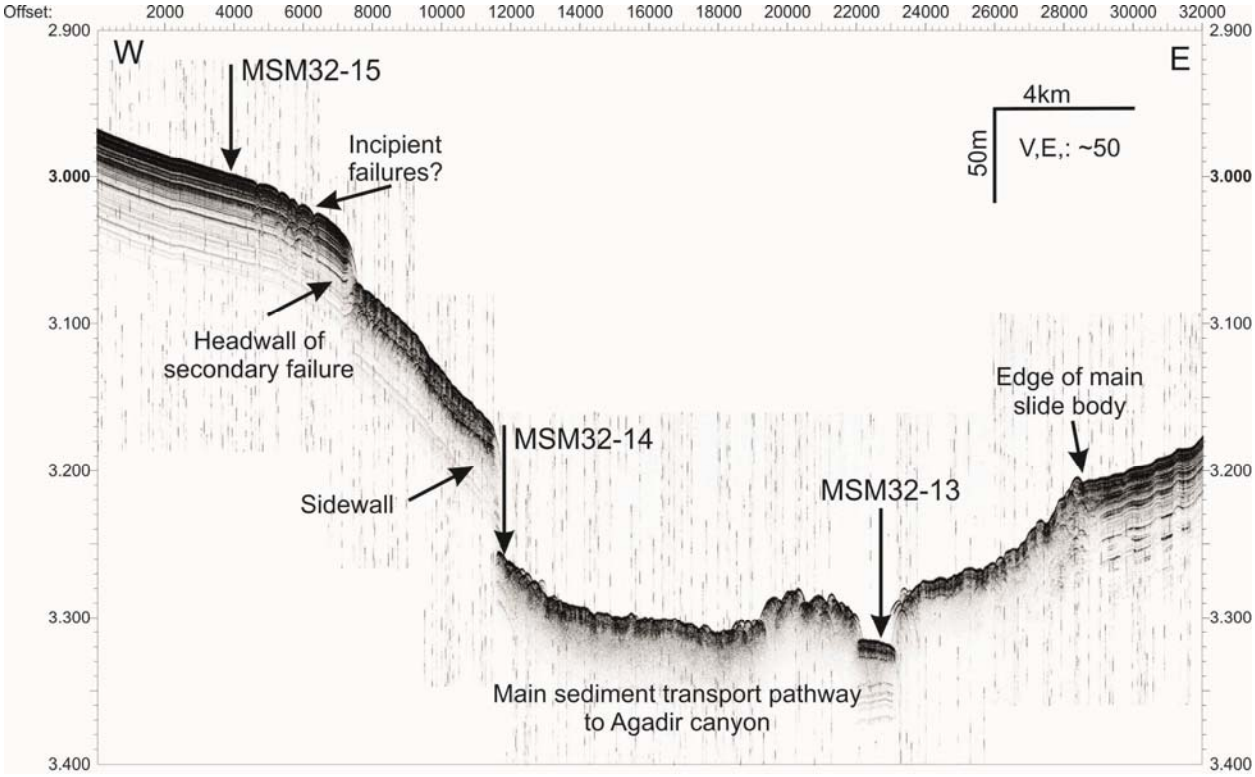

Fig. 9 Parasound profile crossing the main slide fairway south of Agadir Canyon. Gravity cores MSM31-13 to 15 were taken along this profile. Location of profile is shown on Fig. 21.

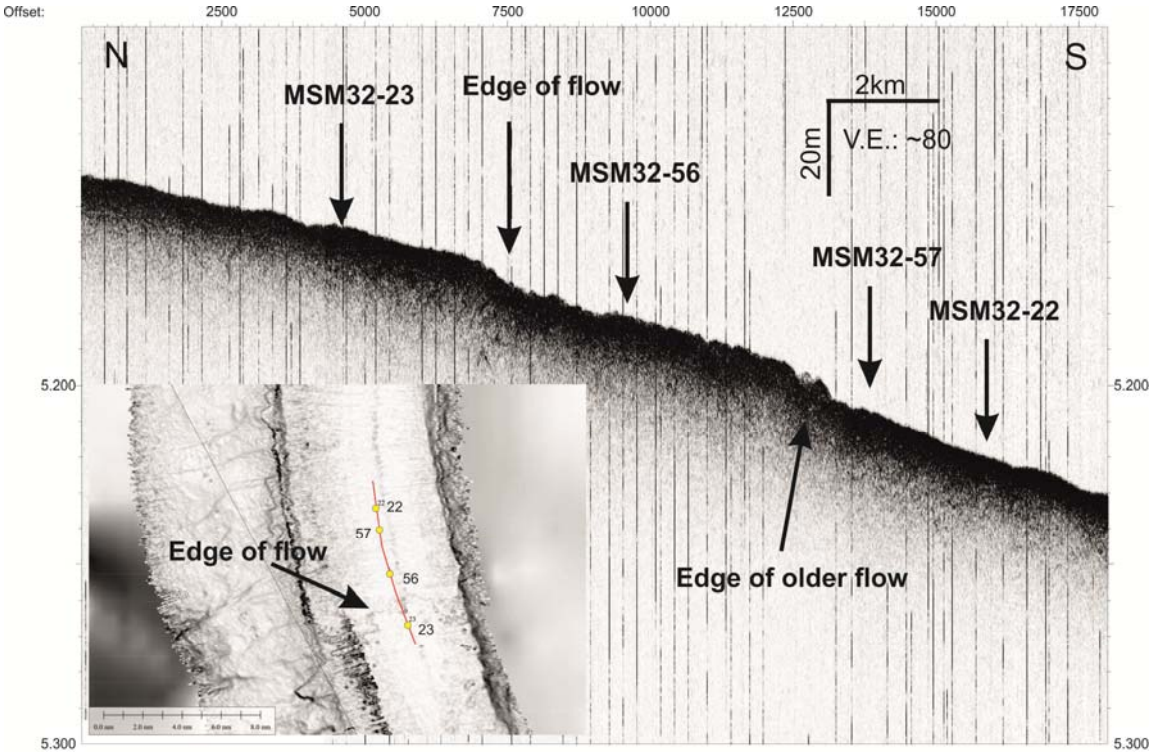

Fig. 10 Parasound profile collected along the thalweg of Agadir Canyon; it shows flow terminations inside the canyons. The small inset map shows the location of the profile. See Fig. 2 for general location of profile.

The sediment slides identified in the fairway mentioned above enter Agadir Canyon in about 2700 m water depth about 120 km off the shelf break. Surprisingly the slides do not mix when entering the canyon but continue to move further downslope inside the canyon. An area with

flow terminations is shown on Fig. 10. This area is ~300 km away from the canyon head. Little breaks in slope indicate the edge of individual flows, which was proven by coring in this area.

Parasound data across the shelf show a great variety of features including basement outcrops, sediment waves, a thin mid shelf mud belt in the area of the Sous River, and isolated small deposition centers. The sediment freight of the Sous River is transported to the north but does not reach the head region of Agadir Canyon; the shelf in the region of Agadir Canyon is sediment starved. Hence, no significant sediment transport from the shelf in the main Agadir canyon is taking place in present times. This may explain the lack of turbidites related to the devastating earthquakes in the Agadir region in 1731 and 1960. Surprisingly no clear indications for incised valleys were found along the entire surveyed shelf. Only one tributary canyon of Agadir Canyon about 100 km north of the head region of the main canyon clearly cuts into the shelf (Fig. 11). A buried continuation of the valley, however, can only be traced for a few km further to the shore. The depression seen on Fig. 11 is a sediment sink while the regions north and south of this depression do not show any significant amounts of Holocene sediments. We assume that this tributary canyon is an important pathway for sediments from the shelf into the Agadir canyon. Several box cores in this region recovered a fine sand, which we were not able to penetrate with a gravity corer.

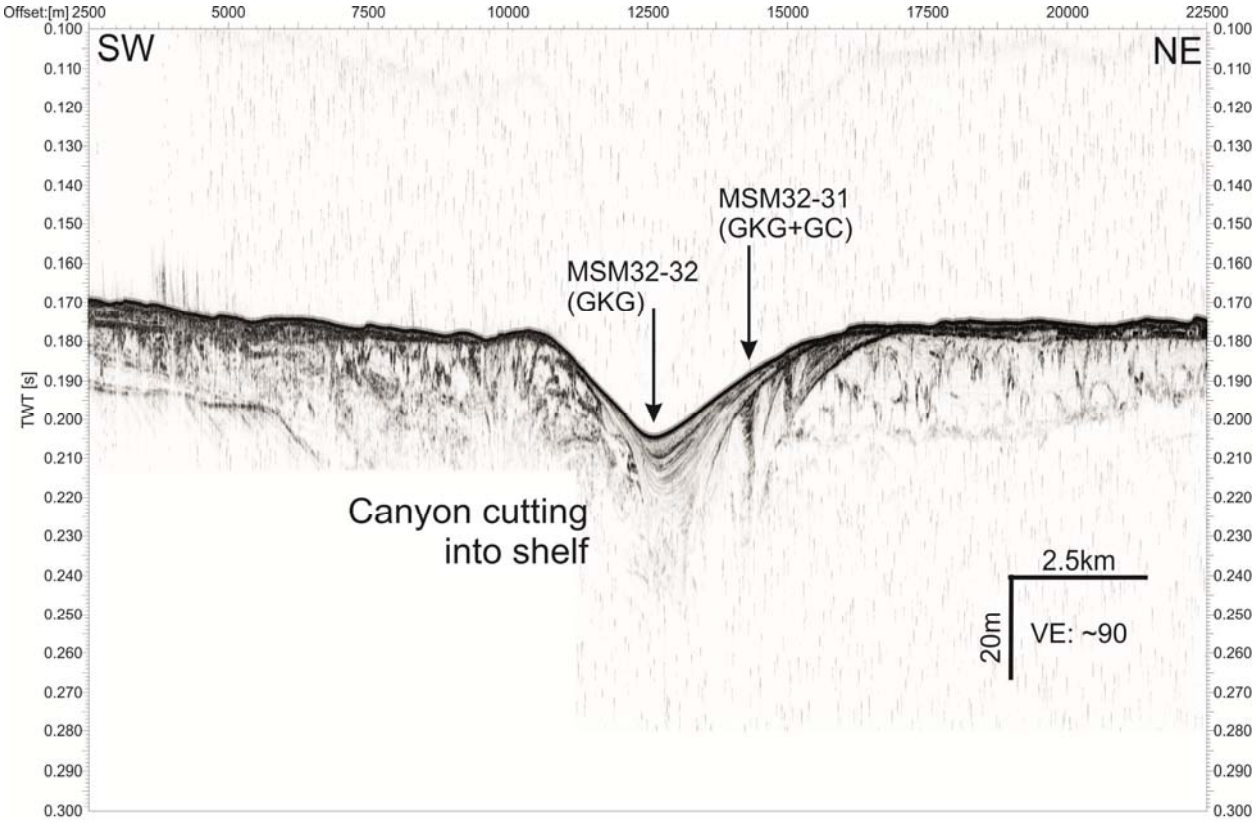

Fig. 11 Parasound profile crossing a tributary canyon cutting back into the shelf. Location of cores (for orientation) is shown on Fig. 2.

Fig. 12 shows a Parasound profile crossing the area of cold-water carbonate mounds north of Agadir Canyon. The bathymetric data (see Fig. 4) shows thousands of individual conical peaks with diameters in the range of hundreds meters and heights of ~10m. The Parasound data show that they are located on both sides of a morphological high. Giant box corers were taken on selected highs based on the bathymetric data. None of these samples is located exactly on a

Parasound line. The systematic sampling approach indicate that dead corals cover the northern flank of the high while living corals were recovered from the southern flank. The Parasound data indicate slight differences between these two areas. The mounds on the northern flank are a bit more subdued as they are partly covered by sediments. The combination of all available data in this area (acoustics, samples and CTD-data) will be used to investigate causes for the occurrence and distribution of life and dead corals.

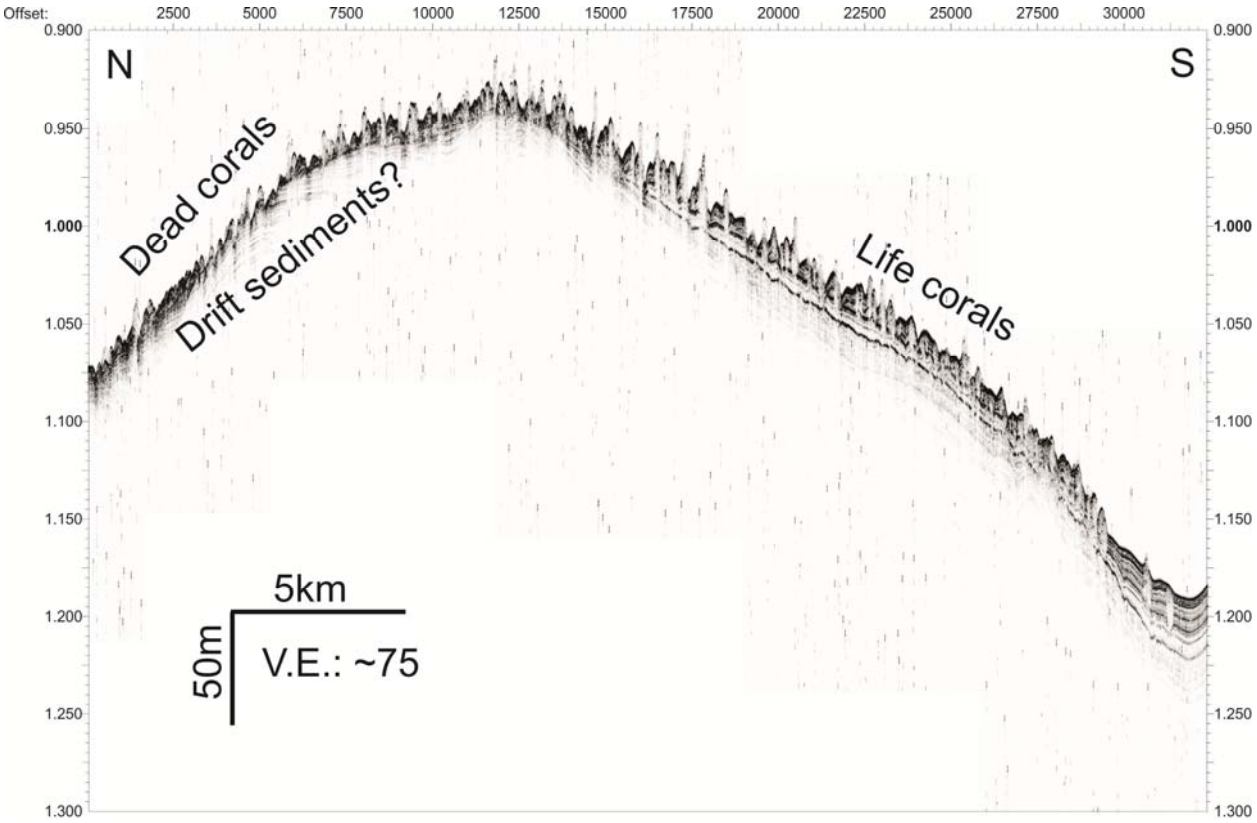

Fig. 12 Parasound profile crossing the carbonate mounds north of Agadir Canyon.

5.2. TOBI-Sidescan Sonar

5.2.1. System description

Towed **O**cean **B**ottom **I**nstrument (TOBI) is an instrumented vehicle, which is towed close to the bottom of the deep ocean from a ship, and uses sound to form detailed images of the sea floor (Felwellen et al., 1993). TOBI was developed by NOC and has been in service since 1990. The TOBI vehicle provides a highly stable platform for the on-board sonars. The vehicle weighs two and a half tonnes in air but is made neutrally buoyant in water using syntactic foam blocks. A 100 m-long neutrally buoyant umbilical connects the vehicle to the 600 kg depressor weight. This in turn is connected to the fiber optic tow cable of RV MERIAN. All signals and power pass through this cable (Fig. 13).

The TOBI system deploys a deep towed dual sidescan sonar system based around 30 KHz. Range to each side of the nadir (central zone) is 3 km, yielding a total swath width of 6 km. The seabed footprint ranges from about 4 x 7m close to the vehicle track to 42 x 2 m at far range. Usually is ‘flown’ about 300 – 500 m above the sea floor. Height above the sea floor is controlled by cable length. Although TOBI's main instrument is a sidescan sonar, a number of other instruments are fitted to make use of the stable platform TOBI provides (7.5 kHz sub-

bottom profiling sonar, magnetometer, and CTD, and a range of vehicle attitude sensors for pitch, roll, and heading). Technical specifications of all used instruments are given in Tab. 1.

Fig. 13 TOBI ready for deployment during Cruise MSM32

Tab. 1: Technical specification of the individual components of TOBI

Mechanical	
Towing method	Two bodied tow system using neutrally buoyant vehicle and 600kg depressor weight.
Size	4.5m x 1.5m x 1.1m (Length x Height x Width).
Weight	2500kg in air.
Tow cable	Up to 10km armoured coaxial cable
Umbilical	100 meters long x 50mm diameter, slightly buoyant.
Tow speed	2.5 knots
Sonar Systems	
Sidescan Sonar	
Frequency	30.37 kHz (starboard) & 32.15 kHz (port).
Pulse	Length 2.8ms.
Ouput Power	600W each side.
Range	3000m each side.
Beam Pattern	0.8 x 45 degree fan.
Bathymetry Sonar	
Transmitter	Uses sidescan sonar.
Receiver	6 hydrophone arrays in 2 housings for each side.
Detection	Single and multi-phase.
Range	Up to 3000m each side.
Profiler Sonar	
Frequency	6 to 10 kHz Chirp.
Pulse Length	26ms.
Output Power	1000W.
Range	>50ms penetration over soft sediment.
Resolution	0.25ms
Beam Pattern	25 degree cone.

Tab. 1 (continued)

Standard Instrumentation	
Magnetometer	Ultra Electronics Magnetics Division MB5L.
Range	+/- 100,000nT on each axis.
Resolution	0.2nT.
Noise	+/- 0.4nT.
CTD	Falmouth Scientific Instruments, Micro CTD.
Conductivity	
Range	0 to 65 mmho/cm.
Resolution	0.0002 mmho/cm.
Accuracy	+/- 0.005 mmho/cm.
Temperature	
Range	-2 to 32° Celcius.
Resolution	0.0001° C.
Accuracy	+/- 0.005° C.
Depth	
Range	0 to 7000 dbar.
Resolution	0.02 dbar.
Accuracy	+/-0.12% F.S.
Heading	Octans6000 fibre optic gyroscope.
Resolution	0.01 degrees.
Accuracy	Better than 0.1°, No latitude limitation.
Pitch/Roll	Dual Axis Electrolytic Inclinometer.
Range	+/- 20 degrees.
Resolution	0.2 degrees.
Altitude	Taken from profiler sonar.
Range	1000m.
Resolution	1m.
Additional Instrumentation	
Light back-scattering sensor	WET labs LBSS
Source	2 x 880nm LEDs
Detector	Solar-blind silicon light detector
Range	~10mg/l
Resolution	0.01% F.S., ~1ug/l

5.2.2. TOBI image processing

Onboard processing equipment during this cruise consisted of a standard PC laptop with a virtual Linux partition and a total of 90 Gigabyte of disk space. All data were archived onto an external 250 Gigabyte hard disk and all final maps onto DVD.

The ship's navigation was recorded online on a server of the ship. The data were transferred on a daily basis and then tested for time-continuity and abnormal speed values. No gaps in the navigation data file occurred. Good navigation data is essential for processing, because the vehicle position and hence the sidescan image position is calculated from it.

The winch data (wireout) were recorded analogue and stored in a separate file. The TOBI imagery was downloaded from the CD-ROMs using a subsample and average factor of 4. This gave a pixel resolution of 3 meters and an almost 2-fold improvement of the signal-to-noise ratio.

During the expedition, a total of six deployments took place. Only on three runs seabed data was collected, the other three deployments had to be abandoned due to technical problems. The three survey runs, were split into areas 1-3, containing a total of 11 blocks (processed in UTM, zone 29) to facilitate processing. The approximate size of the blocks was 0.25 by 0.25 degrees for most areas. After each survey run was completed, the imagery was processed using the PRISM (v5.0) and ERDAS Imagine (v2013) software suites to produce geographically registered imagery, which could then be composed onto a series of map sheets. The individual blocks of each run were mosaicked together to create a single image. This digital version of the imagery of each area was then made available for the onboard Geographical Information System (GIS) Software Global Mapper.

The processing of TOBI imagery has two main phases: Pre-processing and Mosaicking. The pre-processing stage involves correcting of the side-scan sonar characteristics, removal of sonar specific-artefacts and geographical registration of each individual ping. This processing stage is solely composed of PRISM programs and runs from a graphical user interface. The PRISM software uses a modular approach to 'correct' the imagery, which is predefined by the user in a 'commands.cfg' file. For this data it was defined as:

```
suppress_tobi -i %1 -o %0
tobtvg -i %1 -o %0 -a
mrgnav_inertia -i %1 -o %0 -u 159 -n navfile.veh_nav
tobtvg -i %1 -o %0 –h -l 100
tobslr -i %1 -o %0 -r 3.0 , res
edge16 -i %1 -o %0 -m
drpout -i %1 -o %0 -u -f -p -k 201
drpout -i %1 -o %0 -u -f -p -k 51
shade_tobi -i %1 -o %0 -t1,4095
increm –i %1 –o %0
```

To explain this in sonar terms (in order):

- Removal of any surface reflection (i.e. from vehicle to the sea surface and back) – generally only a problem in shallower water depths, where a bright stripe or line is seen semi-parallel to the ship's track. Removal is only done when the imagery is unambiguous, whether the line is true artefact and not an actual seafloor feature. The result can sometimes be seen on the final imagery as a faint dark line.
- Smoothing of the altitude of the vehicle above the seafloor. The altimeter sometimes cannot locate the seafloor, possibly due to very soft sediment thus reducing the return profiler signal. Smoothing is done by a median filter of the given values, comparing this with the first return seen on the port and starboard sides, and applying a maximum threshold for altitude change if first return and altitude value differ. Generally, first return values are used, as these values will be used in the slant-range correction too.
- Merging of ship navigation and cable data with the imagery and calculation of the TOBI position using an inertial navigation algorithm. The 'navfile.veh_nav' file contains ship position and cable values and an umbilical length of 102 meters plus an additional 57 meters for the distance between the GPS receiver and the approximate point where the cable enters the water. The cable values from the shipboard winch system were used in the TOBI cable

file. Various assumptions are applied: the cable is assumed to be straight, the cable value is assumed to be correct, and zero cable is set when the depressor enters the water.

- Uses the TOBI compass heading. A smoothing filter of 100 pings is applied. The heading values are used in the geographic registration process to angle each ping relative to the TOBI position.
- Slant-range correction assuming a flat bottom. This is a simple Pythagoras calculation assuming that the seafloor is horizontal across-track and sound velocity is 1500ms^{-1}. Each pixel is 8ms and generally equates to 6 meter resolution; any pixel gaps on the output file are filled by pixel replication.
- A median filter to remove any high or bright speckle noise. A threshold is defined for the maximum deviation for adjoining pixels over a small area above which the pixel is replaced by a median value.
- Dropout removal for large imagery dropouts. When the vehicle yaws excessively, it is possible for the 'transmit' and 'receive' phase of each ping to be angled apart. If this exceeds the beam sensitivity value (0.8º) little or no signal is received, creating a dark line on the imagery. The program detects the dropout lines and interpolates new pixel values. If more than 7 dropouts are present concurrently (28 seconds) no interpolation is done.
- More dropout removal but for smaller, partial line dropouts. If more than 7 partial dropouts are present concurrently (28 seconds) no interpolation is done.
- Across-track equalisation of illumination on an equal range basis. This assumes that the backscatter from a particular range should average a given amount for each piece of data. The near-range pixels and far-range pixels are generally darker than mid-range pixels. This is due to the transducer's beam pattern and differences in seafloor backscatter response in terms of angle of incidence. The result of this is to amplify the near and far-range pixels by about 1.5 and reduce the mid-range pixels by 0.8.
- Adds a pixel value of 1 to each pixels to avoid zero pixel values that would appear white on a transparent or white background, e.g. when printing maps.

Once these calculations have been applied to a piece of data, the individual pings are placed on a geographic map. To emulate beamspreading the pixels are smeared over a small angle (0.8º) if no other data is present in those pixels. As survey tracks are designed to overlap the imagery at far-range, any overlapping data pieces are placed on separate layers of the same map. This allows user intervention to define the join where one piece touches the other. If small pixel gaps are visible between the geographically mosaicked pings, these are filled with an interpolated value plus a random amount of noise (but having the same variance as the surrounding data pixels).

The second phase (of mosaicking) allows the user to view all the 'layers' of data for an area. The software used is a commercial package named ERDAS Imagine (v2013). Within this software the different layers can be displayed in different colors to distinguish the layers with data that will overlap data from another layer. In order to merge the different layers and their data together, polygons (Areas of Interest –or AOI) are drawn by the user to define the join lines between layers and then applied to create a single layer final image map. This procedure can also be used to remove shadow zones and areas of no data. The program that merges all data within selected AOIs into the final single layer image is called 'addstencil'. This software option was unfortunately not available because of missing file directories. Instead, each layer was processed

as a single image and 'merged' at a later stage using the mosaicking function combined with an image trim procedure to remove unwanted of bad data from the final image. All imagery was geographically registered in a UTM coordinates, zone 29.

Annotation such as ship's track, vehicle track and dates and times can be added to the map. All onboard TOBI sidescan processing is only preliminary due to the short amount of time available. Special care should be taken when trying to identify positions of seabed features as some inaccuracies remain. The data will be processed more thorough back at on land, including true slant-range correction based on the bathymetry dataset available compared to a flat-bottom assumption used aboard.

Tab. 2: Imagery coverage and data sources

Area	Raw disk data	block	Image names
1 (Coral)	740	no. map 10	area1finalmosaic.img
2 (Agadir Canyon)	743-746	nos. map 20-25	area2finalmosaic1.img and area2finalmosaic2.img
3 (Landslide)	748-749	nos. 30-33	area3finalmosaic.img

5.2.3. First results

The first, very short, test deployment took place in a carbonate mound province along the shelf edge. The imagery (Fig. 14) of this almost N-S track shows bright, high-backscatter patches dotted across the seabed. These patches are mound-like features of up to 60 m in diameter and approximately 15-20 m in height, and are clearly distinctive from the lower backscatter matrix that characterizes the surrounding seabed. Several box core samples (Station/sample MSM32-3 and 50 - 55) from the top of nearby mounds contained dead and living coral (sp. *Lophelia pertusa*). Coral framework is known to produce a high backscatter response to most sonar frequencies; hence it can be inferred that the majority of mounds mapped during the TOBI run also contain either living coral or dead framework.

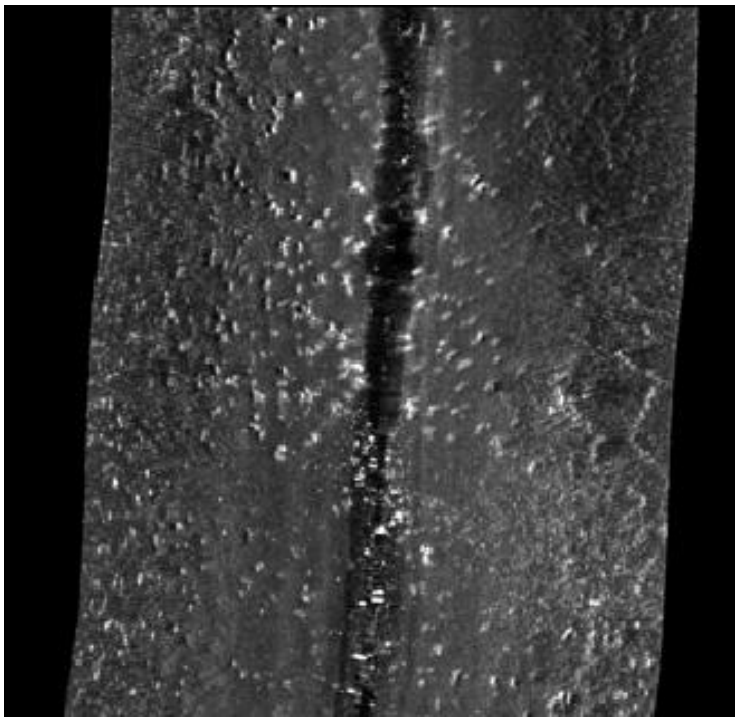

Fig. 14 TOBI run across the carbonate mound province. Bright colors are areas of high backscatter. Swath width is 6km.

The second TOBI run consisted of two parallel lines along the canyon floor axis, from 2600 m down to 3500 m depth. The imagery (Fig. 15) reveals a complex picture of deposits. In some areas the surface is covered by coarser, more sandy deposits (high backscatter – bright colors on the imagery), whereas in others finer, clay-rich material from slope failure deposits dominate (low backscatter – dark colors on the imagery). The axial channel, or thalweg, that cuts through the canyon floor – mainly on the inside bends - appears to be the main transport pathway for the sandy tubidites from the shelf break to the basin floor.

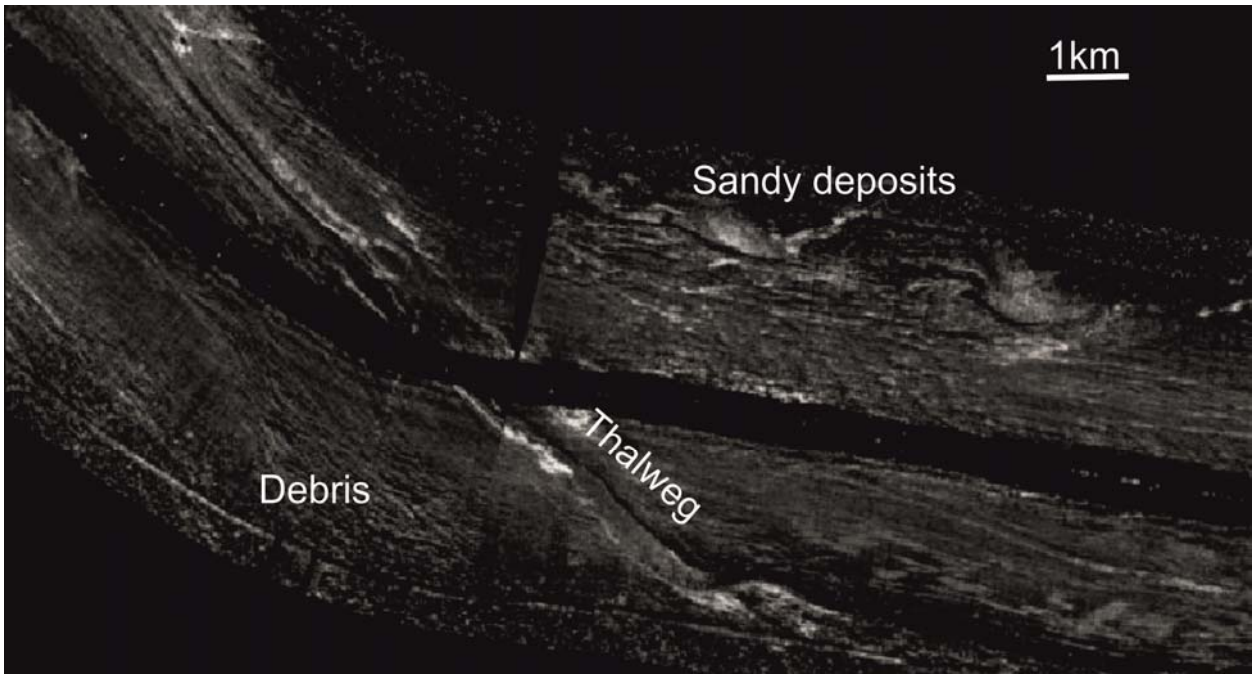

Fig. 15 TOBI run along the axis of Agadir Canyon. Bright colors are areas of high backscatter.

The data also shows deposits from sidewall collapse in the lower part of the canyon as well as slide material from possible bedding-plane failure in upper parts of the canyon. Some of these deposits partly cover the thalweg and, where they do, obscure its route downslope. The final TOBI survey was carried out in the South of the working area. The aim was to map the slope failure deposit pathway and extent, from the headwall downslope. The imagery (Fig. 16) clearly shows two headwalls of about 45 m (direction almost N-S) and 30 m height (roughly E-W) respectively. The sediment above the first headwall has a high backscatter, possibly sandy shelf material. The surrounding sediments below the headwall are very homogeneous and appear in dark gray colors (low - very low backscatter) on the image. This acoustic signature continues for most of the TOBI run, downslope. Sediment cores from the area are dominated by a 5-6 m thick clay-rich drape on top of slide deposits. Further along the run, a few small features, possibly pressure ridges and small morphological steps, occur in the pathway of the slope failure deposits. In addition, a lot of acoustic noise in the mid-to-far range part of the swath appears to blank off any further details. The origin of the dominating noise is unknown but could have been enhanced by the very low backscatter response of the ensonified sediment, in combination with the low angle of incidence.

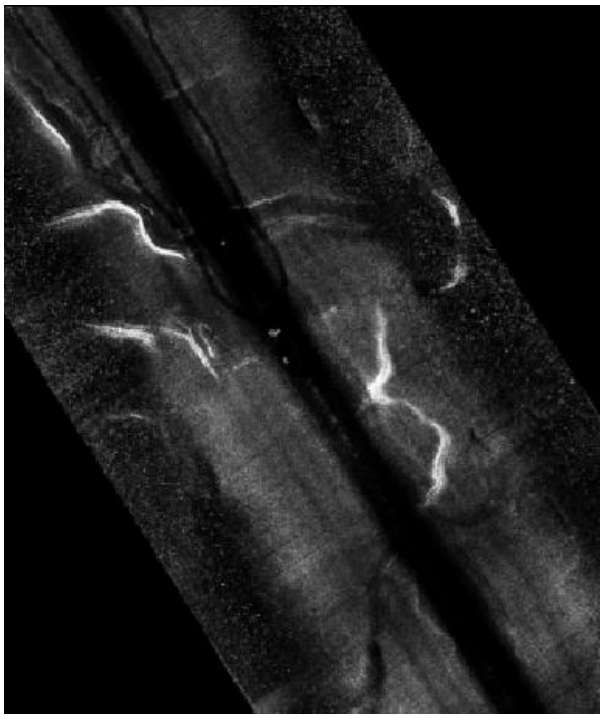

Fig. 16 TOBI run across the headwall area north of Agadir Canyon. Swath width is 6 km. Bright colors are areas of high backscatter.

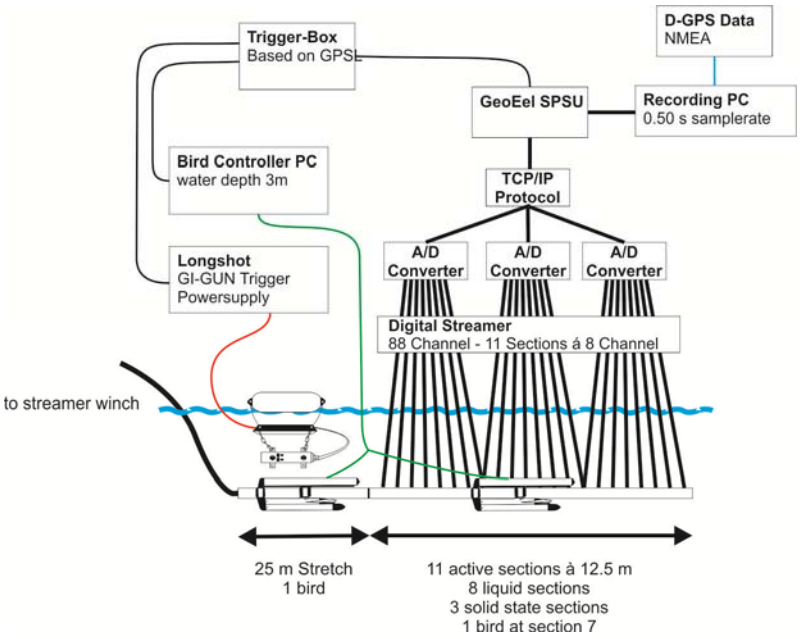

Fig. 17 Setup of 2D-seismic system during Cruise MSM32.

5.3. High resolution 2D multichannel seismic profiling

(S. Krastel, C. Böttner, L. Fu, , S. Hellmann, H. Jähmlich, J. Kretschmer, I. Mücke, A. Schürer)

5.3.1. Introduction

During Cruise MSM32, a Geometrics GeoEel streamer and a standard GI-gun were used to to acquire high-resolution multichannel seismic data. The aim was to resolve small-scale sedimentary structures and closely spaced layers on a meter scale, which can usually not be resolved by means of conventional seismic systems. A 1.7l GI-Gun was used as source during

the cruise. Data were recorded with a Geometrics GeoEel digital streamer. Figs 17 and 18 give an outline of the system setup as it was used during MSM32. Tab. 3 lists the individual setting for each profile. A list of seismic profiles is given in Tab. 5 (Chapter 7).

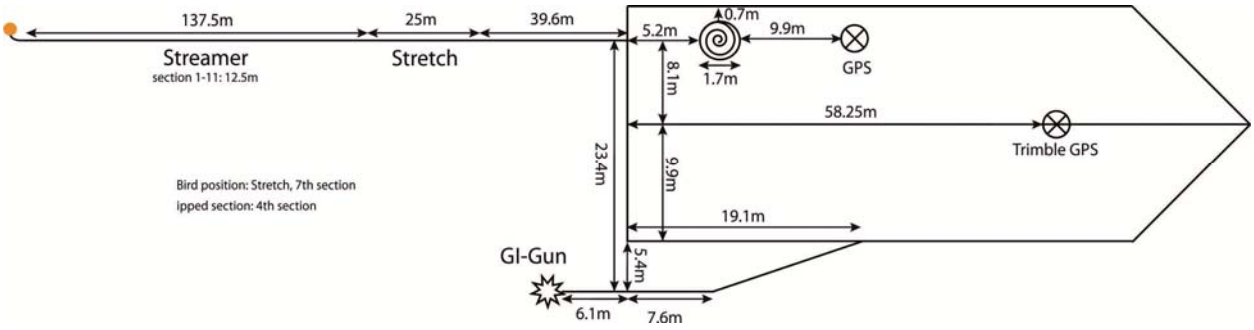

Fig. 18 Deck and seismic gun setting during Cruise MSM32.

Table 3: Source and receiver settings for all seismic profiles.

Profile	Source, mode, shooting rate (s)	Streamer	Birds
P100 1-7	1.7l GI-Gun, harmonic mode, 6s	88 channels, 25m-stretch, Eight 12.5m –fluid section, Three 12.5m solid state sections	Start stretch. Start Section 7
P200 8-13	1.7l GI-Gun, harmonic mode, 6s	88 channels, 25m-stretch, Eight 12.5m –fluid section, Three 12.5m solid state sections	Start stretch. Start Section 7
P300 14	1.7l GI-Gun, harmonic mode, 7s	88 channels, 25m-stretch, Eight 12.5m –fluid section, Three 12.5m solid state sections	Start stretch. Start Section 7
P400 15-20	1.7l GI-Gun, harmonic mode, 7s	88 channels, 25m-stretch, Eight 12.5m –fluid section, Three 12.5m solid state sections	Start stretch. Start Section 7
P500 21-23	1.7l GI-Gun, harmonic mode, 6s	88 channels, 25m-stretch, Eight 12.5m –fluid section, Three 12.5m solid state sections	Start stretch. Start Section 7
P600 24-28	1.7l GI-Gun, harmonic mode, 7s	88 channels, 25m-stretch, Eight 12.5m –fluid section, Three 12.5m solid state sections	Start stretch. Start Section 7
P700 29-32	1.7l GI-Gun, harmonic mode, 7s	88 channels, 25m-stretch, Eight 12.5m –fluid section, Three 12.5m solid state sections	Start stretch. Start Section 7
P800 33-38	1.7l GI-Gun, harmonic mode, 8s	88 channels, 25m-stretch, Eight 12.5m –fluid section, Three 12.5m solid state sections	Start stretch. Start Section 7
P900 39	1.7l GI-Gun, harmonic mode, 6s	88 channels, 25m-stretch, Eight 12.5m –fluid section, Three 12.5m solid state sections	Start stretch. Start Section 7
P1000 40-45	1.7l GI-Gun, harmonic mode, 5s	88 channels, 25m-stretch, Eight 12.5m –fluid section, Three 12.5m solid state sections	Start stretch. Start Section 7
P1100 46-50	1.7l GI-Gun, harmonic mode, 5s	88 channels, 25m-stretch, Eight 12.5m –fluid section, Three 12.5m solid state sections	Start stretch. Start Section 7
P1200 51	1.7l GI-Gun, harmonic mode, 4s	88 channels, 25m-stretch, Eight 12.5m –fluid section, Three 12.5m solid state sections	Start stretch. Start Section 7
P1300 52-54	1.7l GI-Gun, harmonic mode, 5s	88 channels, 25m-stretch, Eight 12.5m –fluid section, Three 12.5m solid state sections	Start stretch. Start Section 7
P1400 55-56	1.7l GI-Gun, harmonic mode, 7s	88 channels, 25m-stretch, Eight 12.5m –fluid section, Three 12.5m solid state sections	Start stretch. Start Section 7

5.3.2. System components

Seismic sources and trigger

During seismic surveying a standard GI-Gun was used as source; it was shot in a harmonic mode (2 * 1.7 l). The GI-Gun was deployed with the starboard side crane and towed ~6 m behind the ship's stern (Fig. 18). The-GI-gun was connected to a gun-hanger with the GI-Gun hanging on two chains 50 cm beneath. An elongated buoy, which stabilized the guns in a horizontal position at a water depth of ~2 m, was connected to the bow by two rope loops. The Injector of the GI gun was triggered with a delay of 40 ms with respect to the Generator signal, which basically eliminated the bubble signal. The gun was shot at 160 bar. Shooting intervals varied between 5 and 7 seconds (depending on water depth) resulting in a shot point distance of 12.5-17.5 m at 5 knots. Shot point distance was significantly smaller while collecting seismic data in combination with TOBI at 2.5 knots. The gun worked very reliable during the cruise. A long shot was used as gun controller. The arming point for the gun was set to 60 ms. The trigger was generated by a custom made unit providing triggers at the full second based on GPS.

Streamer-system

A digital streamer (Geometrics GeoEel) was used for receiving the seismic signals. The system consists of a tow cable (80 m, 40 m in the water), one stretch section (25 m) and 11 active sections (each 12.5 m long). An active section contains 8 channels (channel spacing of 1.56 m for 12.5 m) resulting in 88 channels within the total streamer. The first 8 sections were liquid filled streamers while the last three sections were solid state streamers (see Figs. 17, 18, Tab. 3). One AD digitizer module belongs to each active section. These AD digitizer module are small Linux computers. Communication between the AD digitizer modules and the recording system in the lab is via TCP/IP. A repeater was located between the deck cable and the tow cable (Lead-In). The SPSU manages the power supply and communication between the recording system and the AD digitizer modules. The recording system is described below. Two birds were attached to the streamer (see below). Designated streamer depth was 3 m. A small buoy was attached to the tail swivel.

Bird Controller

Two Oyo Geospace Bird Remote Units (RUs) were deployed at the streamer. The locations of the birds are listed in Tab. 3. All RUs have adjustable wings. A bird controller in the seismic lab controls the RUs. Controller and RUs communicate via communication coils nested within the streamer. A twisted pair wire within the deck cable connects controller and coils. Designated streamer depth was three meters. The RUs thus forced the streamer to the chosen depth by adjusting the wing angles accordingly. The birds were deployed at the beginning of a survey but no scanning of the birds was carried out during the survey because bird scans caused problems with the acquisition system. The birds worked very reliable and kept the streamer at the designated depth.

Data acquisition systems

Data were recorded with acquisition software provided by Geometrics. The analogue signal was digitized with 2 kHz. The data were recorded as multiplexed SEG-D. One file was generated per shot. The acquisition PC allowed online quality control by displaying shot gathers, a noise

window, and the frequency spectrum of each shot. The cycle time of the shots is displayed as well. The software also allows online NMO-Correction and stacking of data for displaying stacked sections. Several logfiles list parameters such as shot time and shot position. Data were converted to SEG-Y file while being at sea.

5.3.3. First results of seismic survey

Preliminary data processing was carried out for all profiles onboard. Several channels of each shot were filtered and stacked. The brute stacks were loaded to a seismic interpretation system (IHS Kingdom Suite) and used for preliminary interpretation. In total, we collected about 1500 km of seismic seismic profiles (see Fig. 2). All data show a very good quality.

Fig. 19 shows the net of profiles in the landslide area south of Agadir Canyon. A profile crossing the main headwall area shows pronounced wavy features (Fig. 20). The wavy features are also visible on the bathymetric data; they show an along-slope strike direction and extend south and north of the failure area (see Fig. 5). The headwall shown on Fig. 20 coincides with the steep seaward-facing flank of a wave suggesting a strong interaction between sediment waves and failure location. The location of the failure seems to be partly controlled by the sediment waves. Slide deposits immediately below the headwalls are very thin. The NW-part of the profile shown on Fig. 20 shows thick (up to 50 m) landslide deposits. The seismic data also show older buried mass transport deposits.

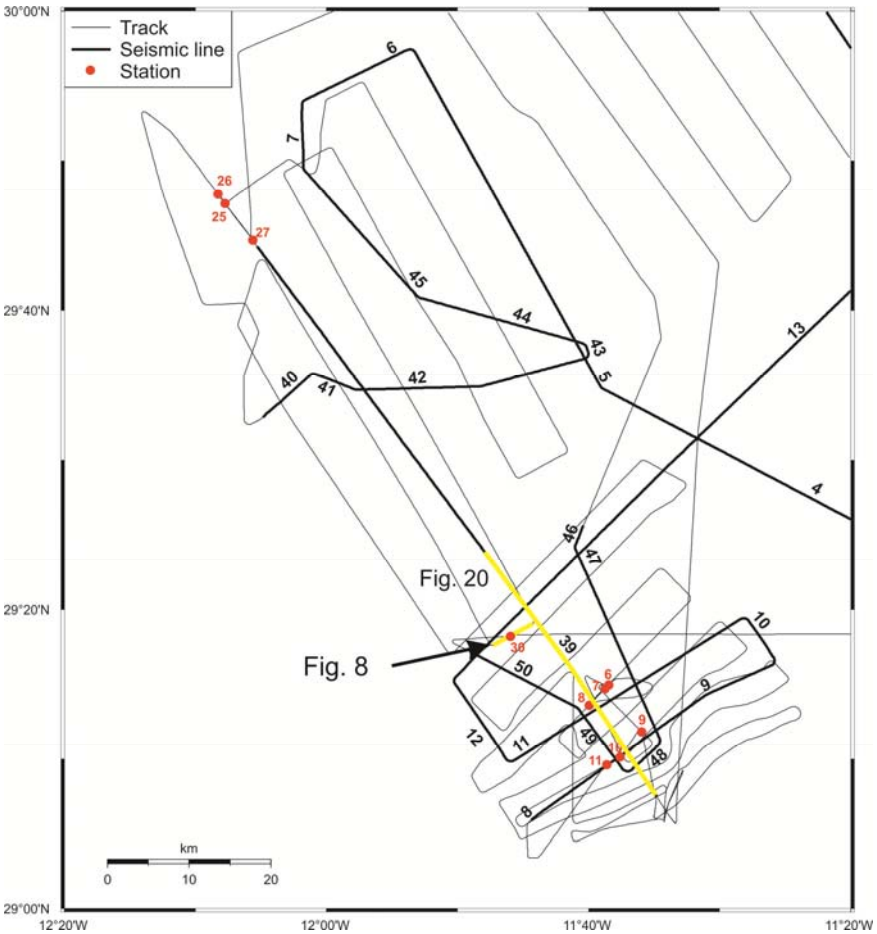

Fig. 19 Track chart showing locations of seismic profiles and cores in the landslide area south of Agadir canyon

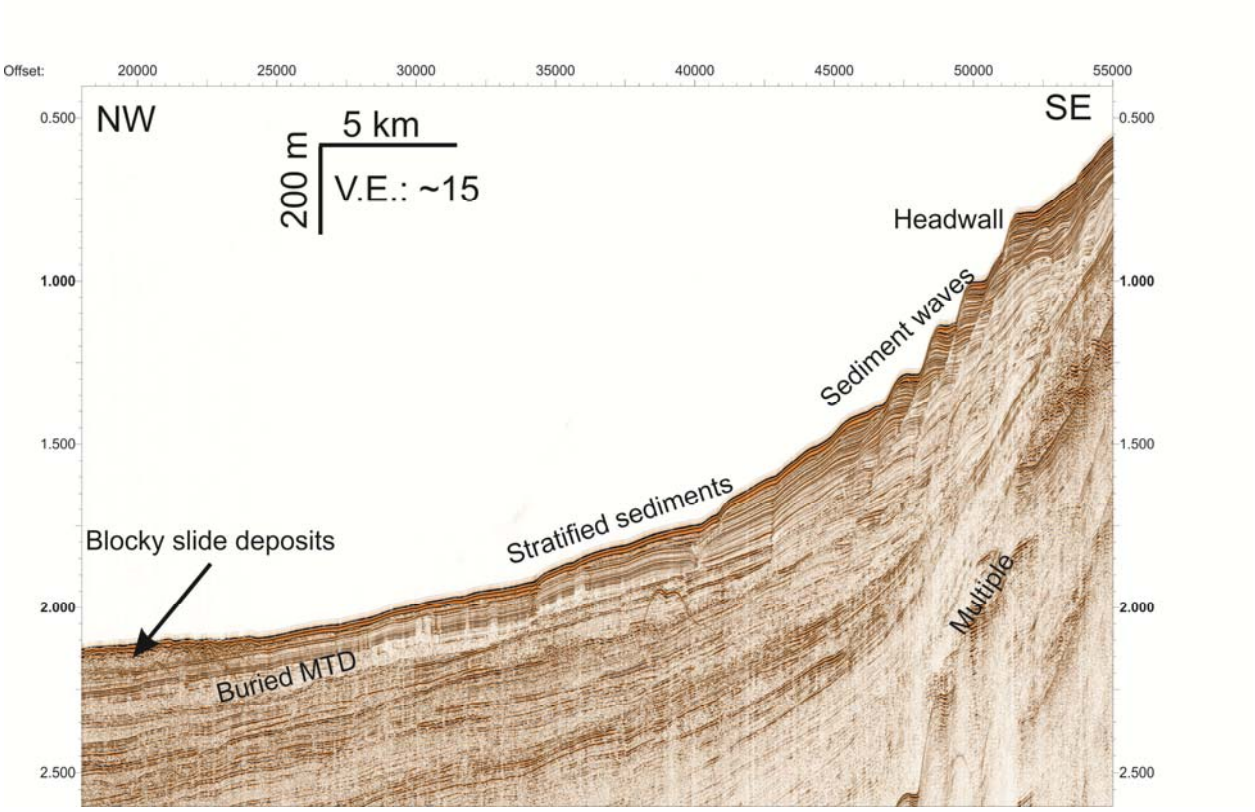

Fig. 20 Brute stack of the upper part of seismic profile 39 crossing the headwall of the landslide area south of Agadir canyon. Location of profile is shown on Fig. 19.

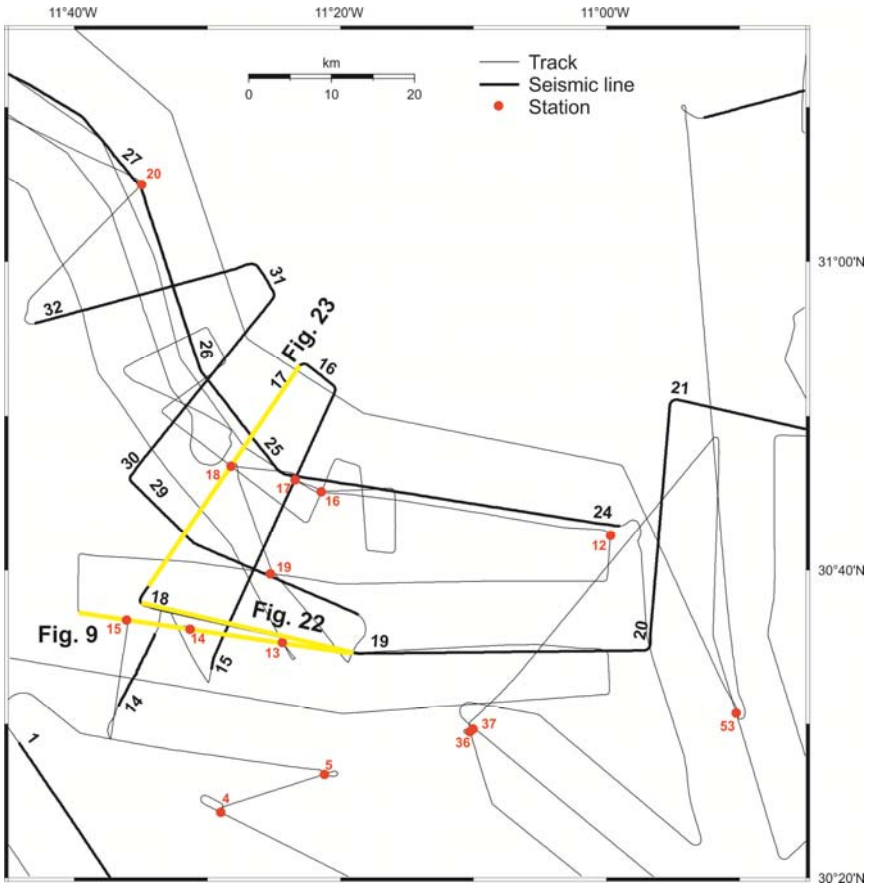

Fig. 21 Track chart showing locations of seismic profiles and cores in the area of the fairway entering Agadir Canyon.

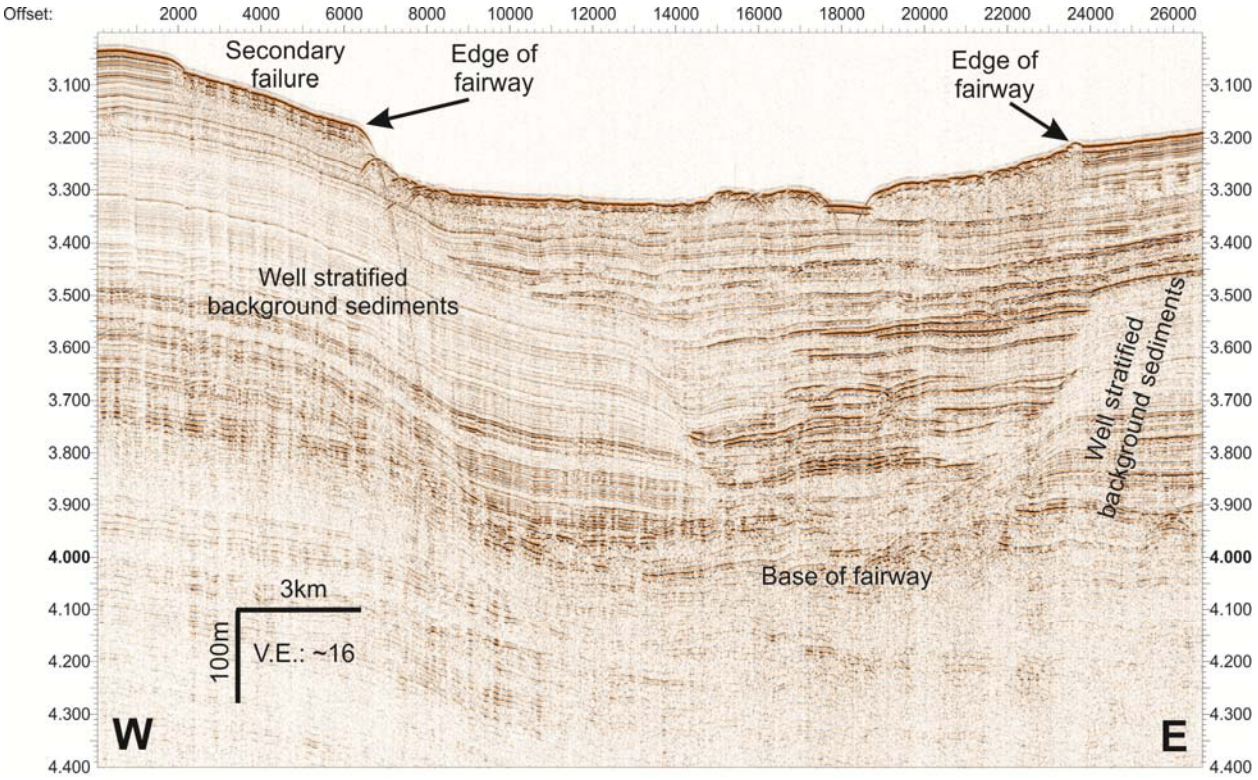

Fig. 22 Brute stack of seismic profile 18 crossing the fairway before entering Agadir canyon. Location of profile is shown on Fig. 21.

The path of the landslide material can be easily followed; it enters Agadir Canyon in the area shown on Figs. 7 and 21. A profile crossing the slide fairway just before entering Agadir Canyon is shown on Fig. 22. The sediments west and east of the fairway are well stratified and mainly undisturbed. A relatively small secondary failure is visible at the western end of the profile. The deposits of the youngest landslide are clearly visible inside the fairway as up to 50 m-thick and about 16 km-wide transparent to chaotic unit. The sedimentary succession beneath the youngest slide deposit shows a disturbed seismic pattern with abundant mass transport deposits of varying sizes down to 700 ms TWT. The disturbed zone narrows to about 10 km in ~ 250 ms TWT subsurface depth. This narrowing coincidences with a slight increase of seismic amplitudes but the general disturbed pattern remains the same. The seismic data suggest a formerly deeply incised fairway, which was subsequently filled with mass transport deposits, turbidites, and hemipelagic background sediments. The fairway has been active for a long time and represents an important sediment transport pathway into Agadir Canyon.

Fig. 23 shows a seismic profile across Agadir Canyon slightly downslope of the location where the fairway enters the canyon. Agadir Canyon is more than 500 m deep at this location and deeply incised in well-stratified sediments. Canyon width is almost 20 km. The canyon floor is relatively flat but slightly inclined to the SE. At least three thick (partly exceeding 80 m) transparent units are imaged beneath the present canyon floor. The seismic data suggest that they represent thick debrite deposits, which entered the canyon via the fairway. Gravity coring allowed sampling the upper most transparent unit. Gravity core 18 (see Fig. 21 for location of gravity core) contains 215 cm of interbedded hemipelagites and thin ‘bypass’ turbidites underlain by sheared and contorted debrite. The contact is erosive and probably represents a significant hiatus. A similar succession of debrite deposits is found on seismic profiles crossing

the canyon further downslope. After entering the canyon, the debris flows continue their way downslope without major indications for flow transformation. First indications for flow transformations are only found ~300 km away from the canyon head (see Fig. 10).

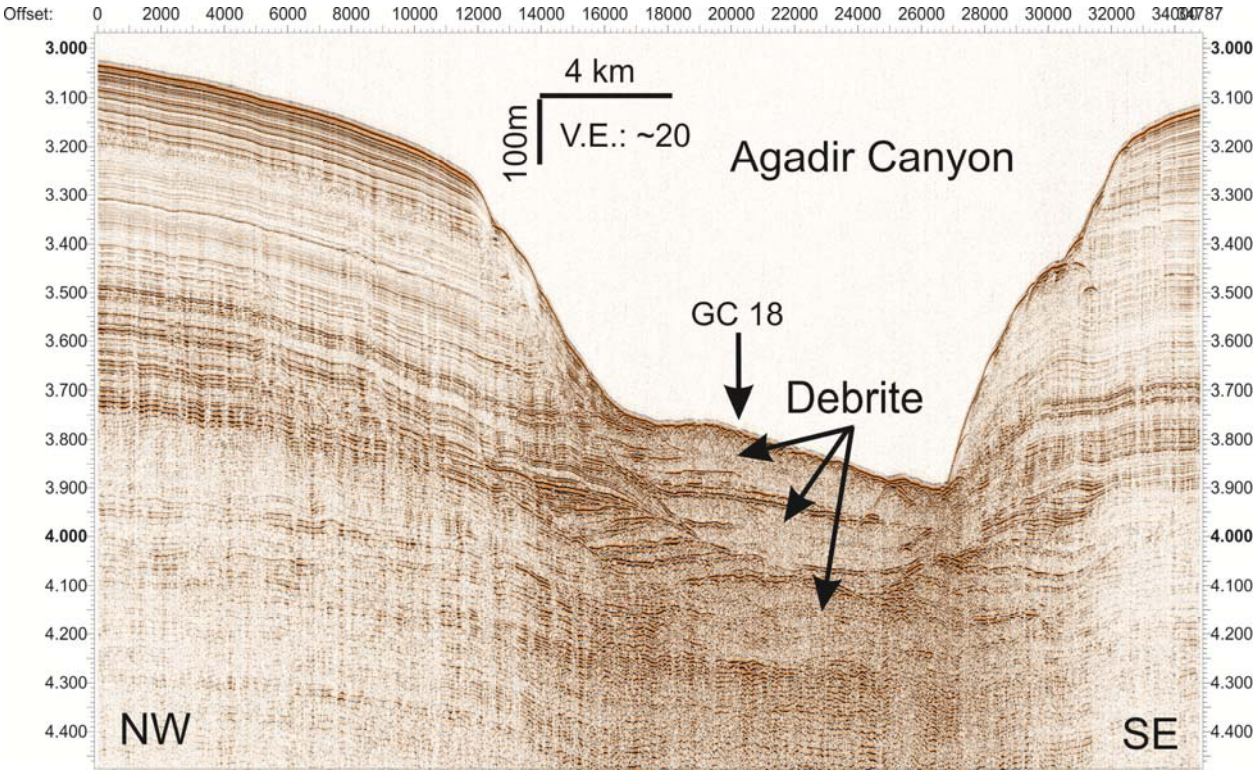

Fig. 23 Brute stack of the upper part of seismic profile 17 crossing Agadir Canyon. Thick debrite deposits are found at the canyon floor. GC 18: Gravity core station number 18. Location of profile is shown on Fig. 21.

5.4. Sediment Sampling

(R.B. Wynn, M. Cartigny, P. Feldens, H. Jähmlich, K. Kraus, M. Schönke, C. Stevenson, D. Unverricht)

5.4.1. Introduction

During cruise MSM32, cores were taken in order to sample gravity flows all over the survey area. In addition, carbonate mounds were sampled for cold-water corals. We used a standard gravity corer and a giant box corer at selected stations. A station list is given in the Chapter 7 (Tab. 4). The core locations are shown together with seismic lines on Figs. 2, 19, and 21.

The Giant Box Corer (GBC) was used in areas, where we expected coarse-grained surface covers and on the carbonate mounds. The Giant Box Corer was applied at 22 stations (Tab. 4). A standard gravity corer was the main tool for sediment sampling. The top weight was 2 tons. During the cruise, 40 stations were sampled using a Gravity Corer (GC) with station-individual lengths of 5 or 10, respectively (Tab. 4). Total core recovery was about 186 m.

5.4.2. Core processing

Gravity corer

After retrieval, the core liners were cut into one meter sections and closed with caps. Each half of the core section was labeled including core depth (starting at the top of the core), MSM-32,

ongoing geology station number and designation for archive (A) and working (W) half. Generally, the top of each core section has yellow caps, while the base has a white cap. Most cores were cut down-core into two halves. The halves were stored in D-Tubes following onboard processing. Few cores were not split, and are to be used for further geotechnical analysis in the laboratory. Due to time constraints, not all core sections could be opened and processed on board. Sub-samples for grain size analysis were taken from the working half every 5 cm to 10 cm, with extra samples as indicated by layers and texture. For most cores, smear slides for nannofossil dating were taken together with the grain size samples. Two to three fall cone tests were done every 5 to 10 cm to determine the undrained shear strength. Extra tests were achieved as determined by layering and texture. For every processed core section, 3 to 7 samples of 2 ml to 7 ml in volume were taken for porosity tests, again according to layering and texture. The porosity samples are stored in water-tight Nunc-sampling tubes. Additionally, sediment resistivity, which is linked to porosity, was measured every 5 cm to 10 cm. An example of undrained shear strength and resistivity measurements is given in Fig. 24. The archive halves were photographed, described in detail and thin slides for the x-radiograph negatives were retrieved.

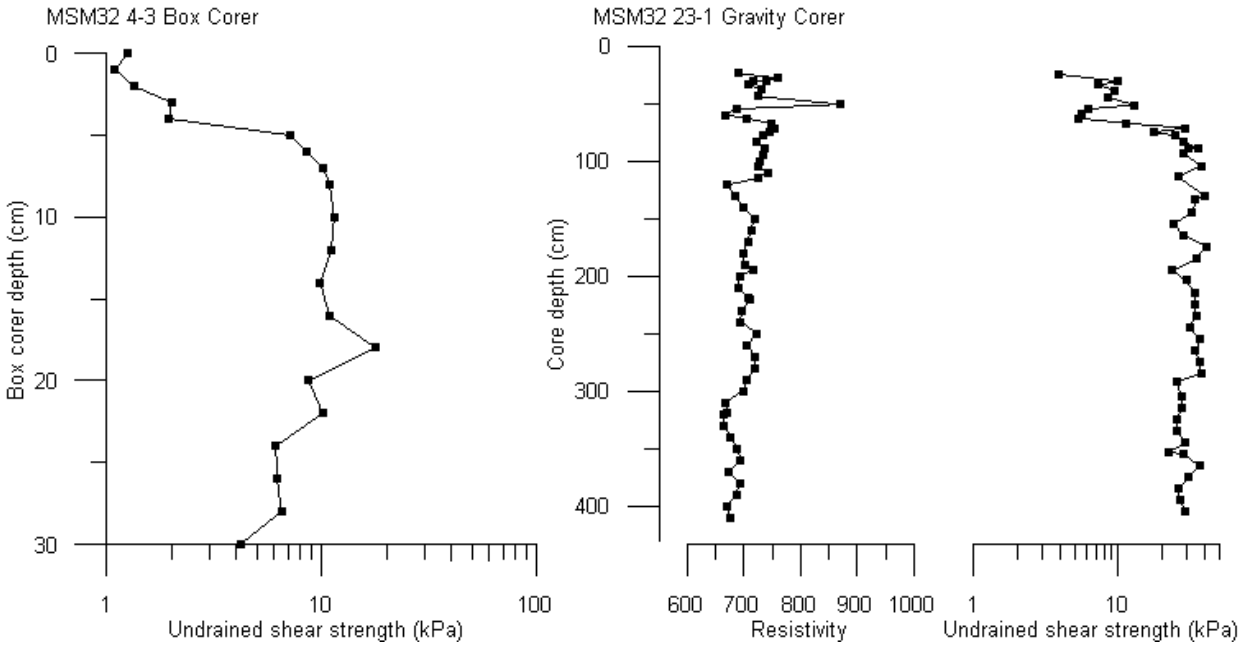

Fig. 24 Left: Measurement of undrained shear strength in a box corer subsample. The first few centimetres of sediment exhibit very low shear strength, with a marked increase at approx. 5 cm depth. Right: Measurements of undrained shear strength and resistivity for core MSM32-23-1. Generally, lower undrained shear strength values correspond with lower resistivities, indicating a higher water content.

Box corer

Following retrieval of the box corer, 4 subsamples were taken, and labeled according to their geological station number. Two metal slides were used to retrieve material for the creation of x-radiograph negatives, to do resistivity measurement and to take porosity samples. Two plastic liners subsamples were labelled and archived, with no further processing done on board. Due to the unavoidable compression of subsamples during retrieval, for few selected box corer shear strength measurements were done within the box corer. Following the surface measurements of undrained shear strength, 1 cm to 2 cm of sediment were carefully removed using a spatula, and

the measurements were repeated. Using this method, undrained shear strength could be measured until approx. 10 cm to 15 cm depth.

5.4.3. Preliminary coring results

The first gravity core of MSM32 was taken on the margin of lower El Jadida Canyon (MSM32-2-1), in an attempt to recover flow deposits in this conduit to Seine Abyssal Plain. Although the acoustic records looked reasonable, the corer was bent and only 1.6 m of interbedded turbidites and hemipelagites were recovered. Stiff pale ooze in the core catcher suggested that an erosional surface was also penetrated.

The second core was a box core (MSM32-2-1) in the coral mound province north of Agadir Canyon, which is described in Chapter 5.5 (together with later box cores, MSM32-45-1 through to MSM32-50-2).

Subsequent gravity and box coring was focused on four main areas: Agadir Slide headwall, Agadir Slide fairway, Agadir Canyon, and Agadir Shelf. These are described in more detail below.

Agadir Slide headwall

A total of six gravity cores were recovered from the Agadir Slide headwall and surrounding areas (see Figs. 2, 19). The first two 5 m gravity cores (MSM-32-6-1 and MSM32-7-1) were taken below the main headwall scar at ~1200 m WD (see Fig. 19 for location) to try and target acoustically transparent 'slide' deposits, but only recovered a sequence of hemipelagic background sediments. Cores MSM32-8-2 (Fig. 25) and MSM32-30-1 (Fig. 8) therefore targeted the glide plane immediately below the western slide sidewall at 1100-1450 m WD, where acoustic records indicated that overlying background sediments were thinner. Both of these cores apparently hit the slide glide plane, represented by very stiff pale sediments underlying draping hemipelagites.

The glide plane was 7.5 m below seafloor in core 8 (Fig. 25), overlain by ~1 m of debrite and a thin sandy suspension fall-out deposit. Over 6 m of overlying background sediments indicated that the slide was probably relatively old (at least tens of thousands of years). In contrast, the glide plane was only ~1 m below seafloor in core 30; overlying background sediments are therefore interpreted to have been winnowed by bottom currents focused along the sidewall at this location.

A core targeting the continuation of the upper headwall further upslope (MSM32-10-1; 640 m WD, see Fig 19 for location)) only recovered background sediments down to ~5 m, indicating that the glide plan was again deeper at this location. A smaller headwall scarp above the main headwall was also targeted (MSM32-9-1; 680 m WD) and recovered an apparent glide plane at ~2.3 m depth that likely represented a smaller, more recent failure. Finally, a core was taken in a slope canyon above the main slide headwall (MSM32-11-1), and recovered a 4 m thick sequence of texturally immature turbidites and muddy debrites, as well as fragments of cold-water corals. It is therefore likely that corals are (or were) present on the canyon walls in this area.

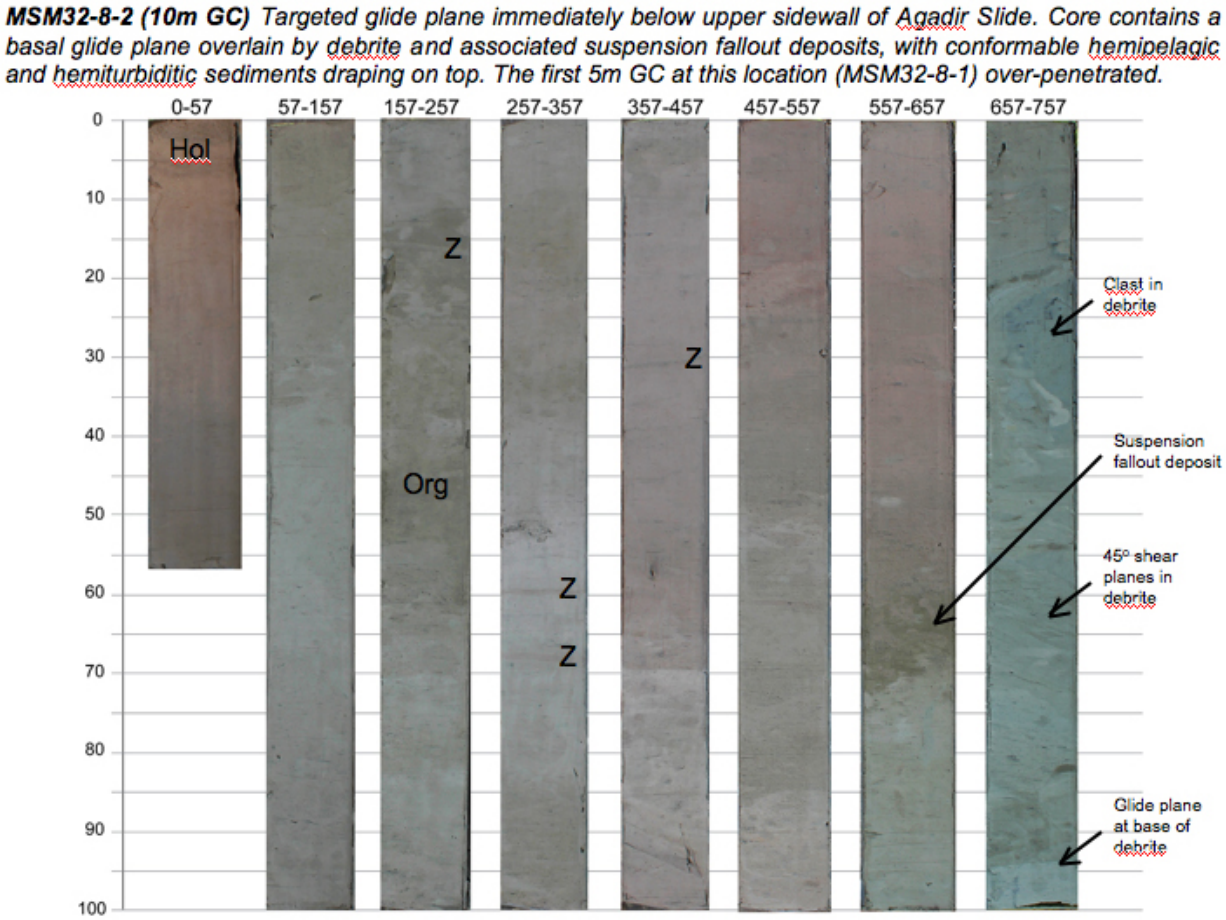

Fig. 25 Photograph Core MSM32-8-2. See Figs and 19 for location of core.

Agadir Slide fairway

A total of 12 gravity cores were recovered from the fairway of the Agadir Slide (see Figs 2 and 21 for locations), mostly using a 10m-long barrel. The average slope angle along the fairway is 0.3°, with water depths ranging from 1900 m at 75 km below the main slide headwall, to 2600 m where the fairway enters Agadir Canyon, ~200 km below the main slide headwall (see Figs 6, 7).

Three cores targeted undisturbed slope sediments adjacent to the slide fairway, in order to provide a litho- and chronostratigraphic record. MSM32-26-1 (Fig. 26) and MSM32-15-1 both recovered ~9 m of background hemipelagic sediments. A lithostratigraphy for the upper 7m was established, based on 13 distinctive correlatable units. Comparison with previous cores taken in the region, particularly in relation to organic- and clay-rich units, indicates that both cores likely extend back ~250 kyrs. Organic-rich units are interpreted to relate to periods of high organic flux, focused on OIS2 (ending at 15 ka), OIS4 (ending at 60 ka) and the OIS5-6 transition (125 ka). A widespread volcaniclastic turbidite in these cores is estimated to be 160-170 ka. This lithostratigraphy will be subsequently validated using coccolith dating. Sedimentation rates in the fairway, based upon these dates, vary from 3.4-5.3 cm per 1000 yrs, with highest rates in the lower fairway adjacent to Agadir Canyon.

Cores MSM32-27-1 recovered obvious slide deposits below 4.7m, with an estimated age of 125 ka. An adjacent core (MSM32-26-1) also targeted apparent slide deposits, based on acoustic records, but initially appeared to contain a record of undisturbed background sediments. However, careful study revealed that the sediment sequence equivalent to the debrite in core 27 was compressed and sheared, indicating in situ deformation by the slide and/or local

remobilisation. Interestingly, a solitary coral found embedded in slope sediments in core 26, adjacent to the fairway, looks to be somehow related to an older landslide event, estimated at 140 ka (see below).

Cores MSM32-28 and 29 were recovered from the middle fairway, and both contain slide deposits at an estimated age of 140 ka. The slide deposit in core 28 contains a similar 'locally remobilised' sediment sequence to that seen in core 26. Slide deposits in both cores are overlain by thin clast-rich sandy intervals, generated by an associated turbidity current. Intriguingly, an older GeoB core (Bremen University) on the southern margin of the middle fairway (GeoB4215) also contains Agadir Slide deposits overlain by a turbidite sand, but also appears to contain an overlying slightly younger debrite estimated at ~120 ka.

Four cores (MSM32-4, 13, 14 and 19) in the lower Agadir Slide fairway all appear to contain the same Agadir Slide deposit as cores 28 and 29, estimated at 140 ka.

MSM32-26-1 (10m GC) *Targeted slope beyond northwest margin of Agadir Slide. Core contains interbedded hemipelagic slope sediments, with a solitary coral at 500 cm (equivalent to the depth of the adjacent debrite) and a single volcaniclastic turbidite at 575 cm.*

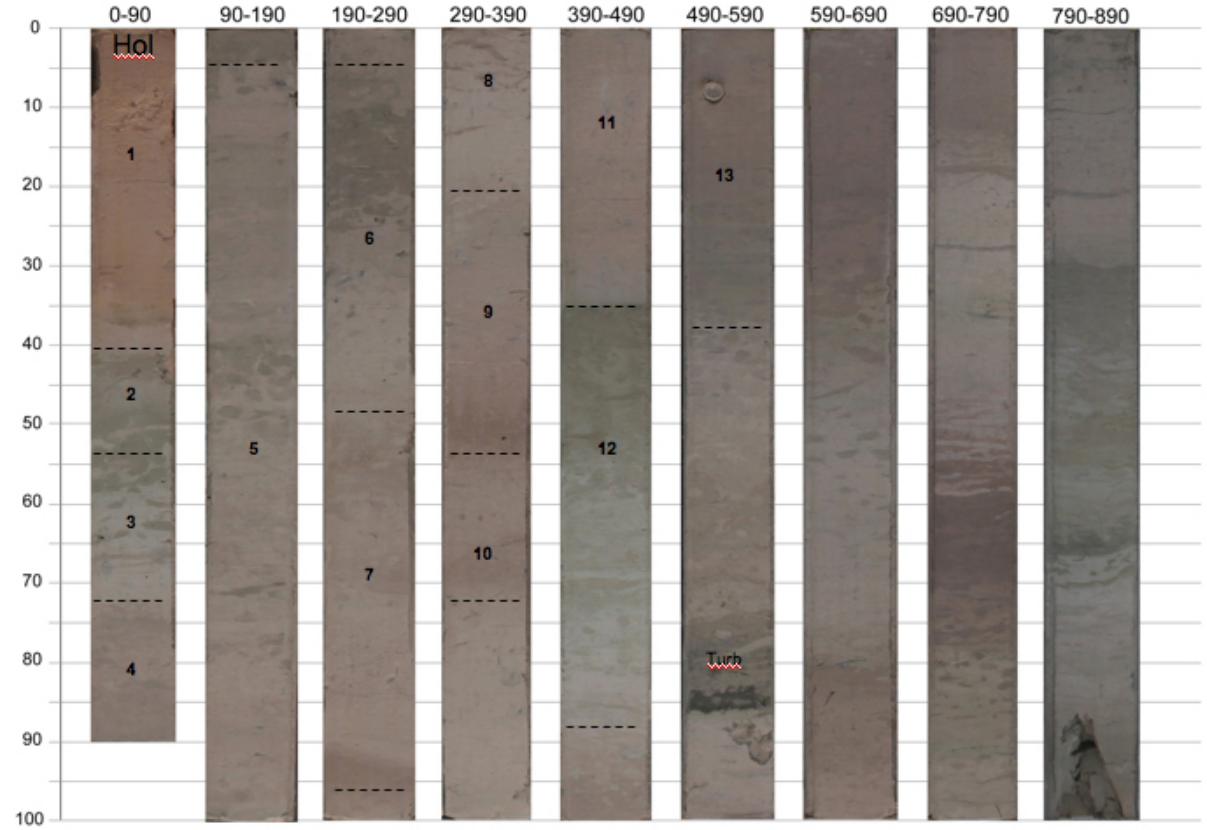

Fig. 26 Photograph Core MSM32-26-1. See Figs. 2 and 19 for location.

Agadir Canyon

Three cores were recovered from upper Agadir Canyon, above the level where the Agadir Slide enters the canyon from the south (see Figs. 2 and 21 for location). Core 16 targeted the main canyon thalweg and recovered two relatively young erosive turbidites, one of which contained large cobbles >8 cm across. Core 37 targeted a 100m-high terrace in the lower reaches of a sinuous tributary canyon, but only recovered 1.3m of sediments after hitting an apparently hard layer. Core 53 was taken ~350m up on a slope adjacent to the main canyon, in the hope of recovering the upper parts of large flows passing through the canyon. The core contains ~8 m of

hemipelagic sediments going back to 140 ka, and a single gravel- and clast-rich erosive sandy turbidite at 4 m depth that apparently corresponds to Agadir Bed 5 at 60 ka.

Cores 17, 18, 20 (Fig. 27), 54, 21 and 55 were taken in a transect down the canyon below the Agadir Slide fairway entrance, and all contain sheared and contorted debrite deposits overlain by an erosion surface and interbedded erosive turbidites and hemipelagites.

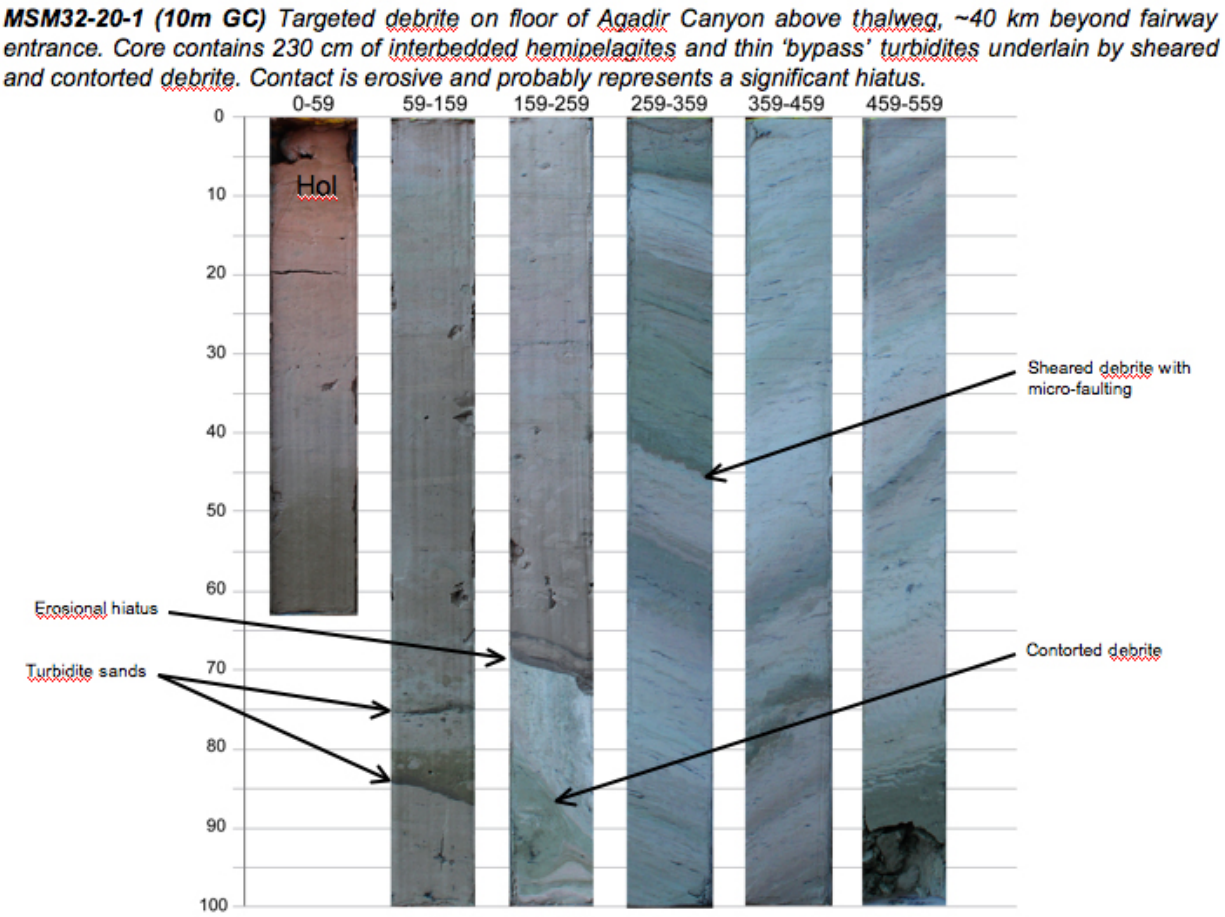

Fig. 27 Photograph Core MSM32-20-1. See Figs 2 and 21 for location.

Only one core (54, located on the canyon floor 100 m above the thalweg) apparently penetrated the base of the debrite, at a depth of 5 m. This may help tie the age of the debrite in the canyon with that in the lower fairway (140 ka). This core also contains indications for basal mixing of the layered cohesive debrite with underlying canyon-floor sands and gravels, leading to formation of a grey, poorly sorted, mixed layer.

This grey mixed layer becomes dominant in cores 23 (Fig. 28) and 56 taken further downstream in the canyon, where two debrite snouts are visible on acoustic data and where slope decreased from ~0.4° to 0.2° (see Fig. 10). In both cores the mixed layer debrite is overlain by an erosion surface and interbedded turbidites and hemipelagites. Cores 57 and 22, taken beyond the toe of the lower debrite snout, contain a thin Holocene drape overlying near-vertically bedded debrite that is interpreted to be the distal section of an older exhumed debrite body.

The presence of debrite in cores extending down the canyon for over 180 km is consistent with seismic data showing subsurface debrite bodies extending all the way to the Agadir Canyon mouth. These data indicate that successive Agadir Slide events did not mix upon entering the canyon, despite slope angles increase to >1° at the fairway termination.

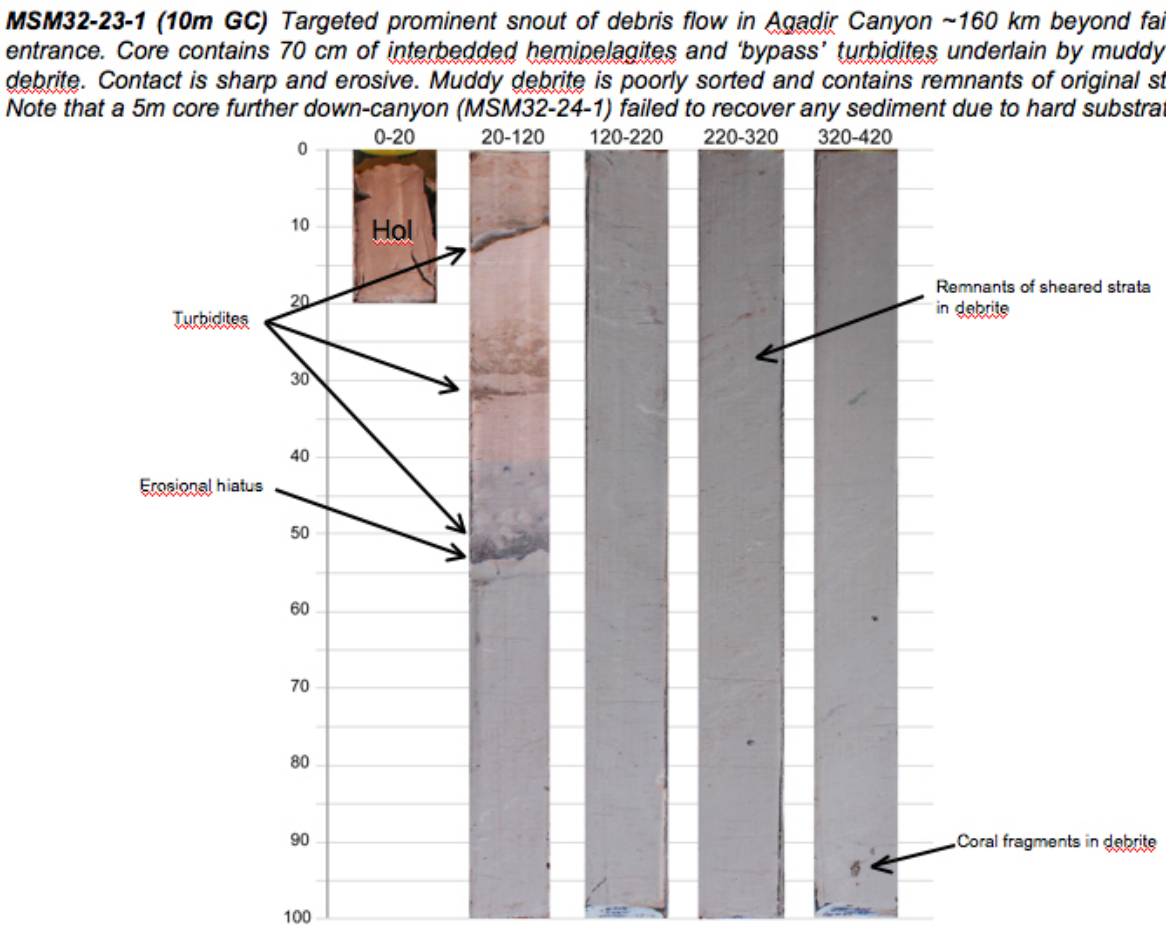

Fig. 28 Photograph Core MSM32-23-1. See Figs 2 and 10 for location.

Agadir Shelf

Gravity coring attempts on the shelf aimed at sampling centre and rim of a canyon forming a conduit from the shelf area to Agadir Canyon (see Fig. 11). However, the canyon, whose morphological onset could be identified at approx. 200 m water depth appears to be filled with a mixture of compact clayey to fine sandy sediment that could not be penetrated to sufficient depth with a gravity corer. Therefore, box corer samples were retrieved from the canyon to identify sediment accumulation rates, surficial sediment composition as well as erosive unconformities in the upper part of the sedimentary sequence.

Next to the incised valley, several box corers and gravity corers were retrieved along the mid-shelf. One aim of these stations was to penetrate presumed Holocene sediments to retrieve older sediments for dating purposes. Unfortunately, due to the sediment properties, penetration depths were not sufficient to sample the inferred pre-Holocene sediment. A further aim was to sample Holocene sediments, both in and outside of the mid-shelf mud belt to determine accumulation rates and estimate the amount of material transported towards the Agadir Canyon. The preliminary interpretation of box corer and Parasound data indicates that large parts of the shelf off Agadir is sediment starved, and that little to no sediment is transported into the head of Agadir Canyon.

5.5. CTD, water sampling and cold water corals

(S. Glogowski, J. von Reumont)

5.5.1. Introduction

The eastern Atlantic Ocean bordering NW Africa and specifically Morocco is known for extensive coastal upwelling, which has been described in Morigi et al. (2001). The indication and description of the complex water mass structure is summarized in Sarnthein et al. (1982). The distribution of the major water masses of the surface layer is coupled to the upwelling-circulation. Accordingly to Sarnthein et al. (1982), there are different water masses upwelling in the northern and southern region (Mittelstaedt, 1991). It needs to be mentioned that the identification of the water mass structure within the working region is derived from only two CTD casts deeper than 2000 m and needs to be considered with caution due to the high variability in time and space.

5.5.2. CTD/Rosette water sampler casts

The main objective of CTD measurements during cruise MSM 32 was to determine general water mass characteristics and particularly the physical parameters of water masses bathing (living) cold-water corals in the Agadir Canyon region off Morocco. Special attention has been given to the assessment of water mass variability in the ultimate vicinity of cold-water coral habitats in time (tidal cycles) and space (locally-regionally). Bottom water samples were taken at all stations to get an overview of the geochemical characteristics of these water masses. In addition, sound velocity data were provided for hydroacoustic mapping.

The deployed Conductivity-Temperature-Depth (CTD) system comprised a Seabird “SBE 911 plus” underwater unit with a set of 24 x 10 l FreeFlow water samplers and automatic release and a Seabird “SBE 11 plus V2” deck unit. Apart from the standard setup, the underwater unit was equipped with two dissolved oxygen sensors, a turbidity sensor and an altimeter. For analysis and interpretation of the measurements, the downcast raw data were processed with “SBE Data Processing” software. For visualization of acquired data we used “Ocean Data View” Version 4.5.3 (Schlitzer, R., Ocean Data View, http://odv.awi.de, 2013). Instrumental oxygen measurements were validated with results from iodometric titration of corresponding water samples. We performed 25 single casts and a yoyo-CTD with repeated casts over 14 hours covering one complete tidal cycle.

5.5.3. Shipboard analyses

The measurements of the CTD oxygen sensors were validated on board with water samples by iodometric WINKLER-Titration after Graßhoff (1983). Water samples were taken during the upcast only. When a designated sampler bottle was released, the oxygen sensor readings were noted and later compared to the titration results. Immediately after collection, the water samples were filled into volume-calibrated WINKLER bottles. Two parallel samples were taken, and we paid particular attention on not having any air inside the WINKLER-bottles. The oxygen was fixed with 0.5 cm^3 manganese-II-chloride and 0.5 cm^3 alkaline iodide. Then the bottles were shaken and stored cool for several hours. Before titration, the manganese hydroxide was solved with 1 cm^3 H_2SO_4 (9M) and the bottles were shaken again. The samples were each transferred into a 250 ml beaker, where they were titrated with 0.02 M sodium thiosulfate until the solution

turned into yellow. After adding 1 cm^3 of zinc iodide solution, the titration was continued until the blue color of the sample disappeared. The factor of the thiosulfate solution was determined with a standard. The oxygen content was calculated from the thiosulfate consumption by using the following standard formula:

O2 = (a * f * 0.112 * 103) / (b-1) [ml/l]
a = consumption of thiosulfate solution [ml]
b = volume of WINKLER bottle [ml]
f = calibration factor of the thiosulfate solution

A total number of 17 titrations was performed. The oxygen contents range from 2.99 to 4.89 ml/l.

Figure 29 shows the comparison between dissolved oxygen contents of CTD and Winkler-Titration for all measurements. The correlation high (R = 0.90) and the resulting formula

CTD_{oxy} [ml/l] = 0.6788 x $Titr_{oxy}$ + 0.7122

was used to calibrate the CTD data.

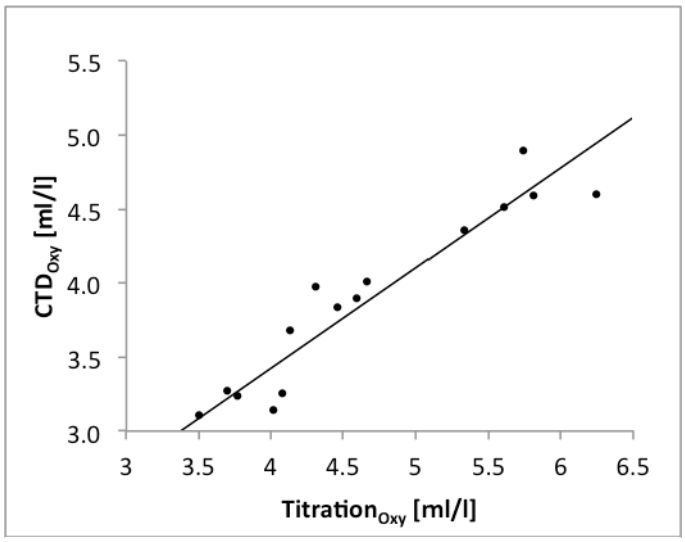

Fig. 29 Comparison of oxygen measurements from CTD and Winkler-Titration exhibits a high correlation. Regression was used for calibrating CTD data.

5.5.4. First results

The overall performance of the CTD system was satisfactory. The recording unit and computers worked without major problems. In general, the up-cast profiles showed a deviation from the downcast profiles in a hysteresis-like manner and thus did not exactly replicate the downcast measurements. The main focus of investigations was to gain data on oceanographic variability in the vicinity of carbonate mound structures, where live or dead cold-water corals were found in box corer samples.

Station MSM32-3-2/ CTD 2 (Fig. 30)

This station was taken at a mount, where living *Lophelia pertusa* were sampled in a box corer (Fig. 31). The uppermost part of the water column down to 52 m comprises the shallow water mass of the upper surface layer which may be influenced by the Surface Canary Current Water

(SCCW) with the lowest salinities around 36.31 psu shallower than 50-60 m. The salinity maximum values in between 99 and 117 m water depth range from 36.35 to 36.36 and are characteristic for the North Atlantic Central Water (NACW), which reaches up north into the Agadir region. The NACW is a subsurface water mass with moderately temperatures of 16.45°C and density value (sigma-theta) around 26.7 kg/m^3. Deeper, around a water depth of 704 m, the salinity minimum of the CTD-cast of 35.46 psu is found. It might be attributed to the onset of the Mediterranean Outflow Water (MOW) as it is characterized by its high salinity combined with relatively high temperatures 9.88°C and a determined oxygen-content of 3.14 ml/l. The potential density value for the living *Lophelia pertusa* in this area reaches 27.33 kg/m^3 (Fig. 30).

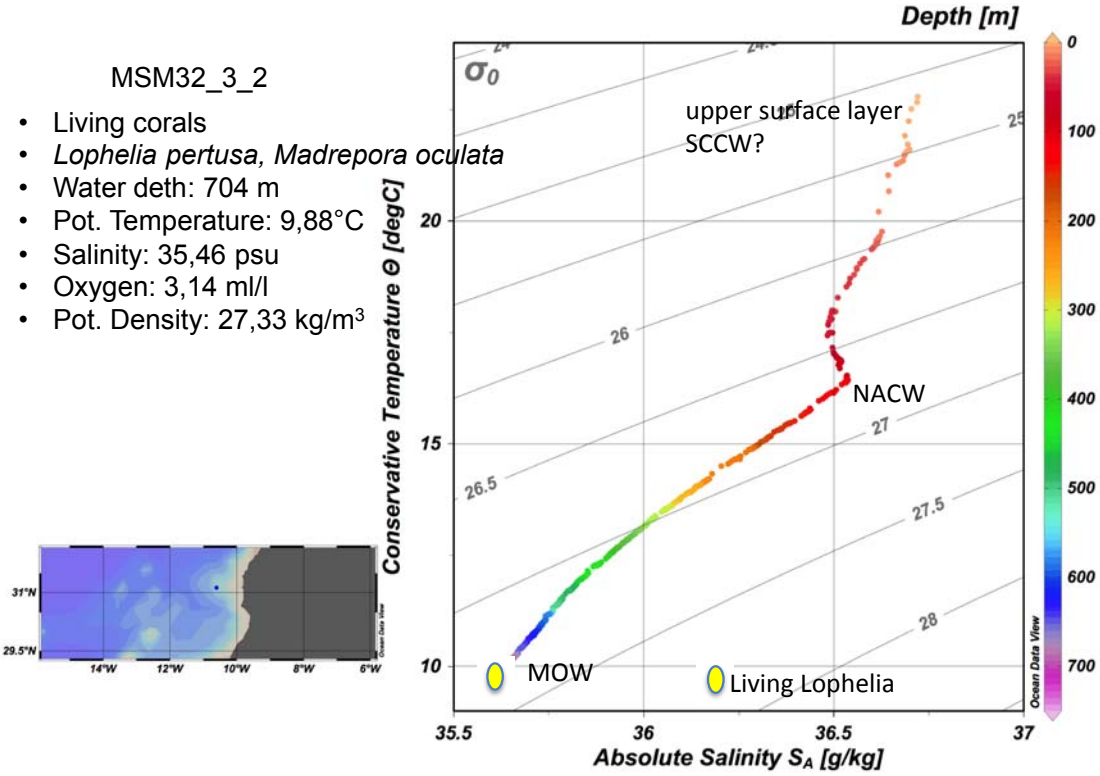

Fig. 30 Temperature-Salinity plot of station MSM32-3-2 on top of a mound with living *Lophelia pertusa* and *Madrepora oculata*. See Fig. 2 for location of station.

Fig. 31 Box corer at Station MSM32-3-2 showing living cold water corals. See Fig. 2 for location of station. Picture: Heiko Jähmlich.

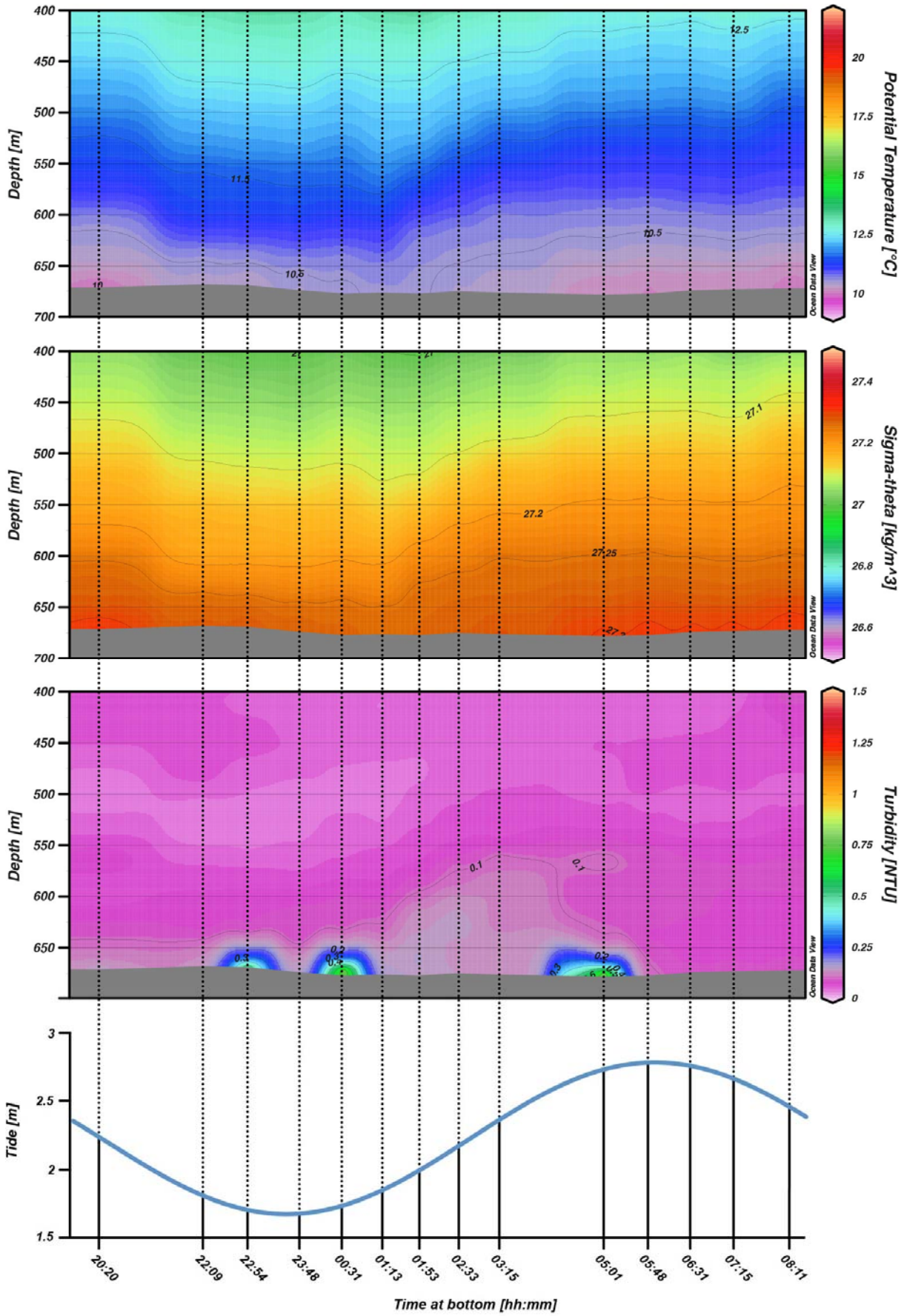

Fig. 32 Yo-Yo-CTD from collected at 25/26.10.2013 (Station MSM32-51). The plots show profiles of temporal variability of potential temperature (°C), sigma-theta (kg/m^3) and turbidity (NTU) at water depth from 400-678 m. Tidal height forecast based on tidal curve for Agadir is shown at the bottom.

Station MSM32-51-2-15/ yoyo-CTD

Additionally we performed a Yoyo-CTD on a site of living cold-water corals with repeated casts over 14 hours on the same position covering one tidal cycle from low tide to high tide. The results for potential temperature (°C), sigma-theta (kg/m^3) and turbidity (NTU) are summarized in Fig. 32. All of the depicted parameters show vertical variability throughout the tidal cycle indicating vertical motion of the water column. From the turbidity data, a horizontal component of motion expressed by the settling and resuspension of sediment can be observed.

For this station the water column clearly reflects the influence of the tidal cycle down to 700 m. Lowest values in potential temperature are observed at low tide in the bottom water with 9.99-10.52 (°C). (Fig. 32). Density sigma-theta increases from ca. 27.0 kg/m^3 in 400 m water depth and decreases to around 27.3 kg/m^3 in the bottom layer. The observed highest values in ca. 700 m water depth at the bottom layer seems to correspond to the water depths where living cold-water corals have been observed (Dullo et al., 2008).

Observations have shown that turbidity reaches highest values around slack water in the bottom layer from approx. 560 m water depth down to the seafloor. However, turbidity shows highest variability of all measured parameters during the course of the 14-hour CTD observations (Fig. 32).

5.6. AquaPAL sensor

(D. Meier, D. Voss)

Within the BMBF funded project AQUAPAK (FKZ 13N11963) a reagent-free optical sensor for the detection of dissolved and emulsified oil constituents (especially PAHs - polycyclic aromatic hydrocarbons) in turbid media will be developed. Existing oil monitoring systems, especially for ship applications (bilge water) mainly detect undissolved oil constituents, e.g. via light scattering. Even after treatment with oil separators discharged waters still contain dissolved PAHs. A reversible, ambiguities-independent and reagent-free sensor for the quantitative detection of dissolved and emulsified oil constituents will offer a great advantage with respect to upcoming environmental awareness, supporting already existing oil monitoring systems, eliminating and minimizing false alarms from water containing scattering particles. With the improved measuring principle even low concentrations of toxic PAHs can be detected. The project is currently in its final phase with a long-term field application on the MARIA S. MERIAN for validation.

On the transit from Bremen to Southampton (24 - 27.09.2013) the newly developed AquaPAK sensor system was installed at the bilge water separator of the MARIA S. MERIAN. During the cruise, three test runs with de-oiled bilge water from the separator were performed (Fig. 33). Hereby, training on the sensor system for the crew was possible because the system will remain on the ship until February/March 2014, with operation in defined time-intervals.

Fig. 33 Turbid sample water of the Maria S. MERIAN after treatment with bilge water separator (left); AquaPAK system with newly developed sensor and reference sensors, installed at the bilge water separator of the MSM (middle); briefing for operation of system (right).

6. Ship's Meteorological Station

There was no meteorologist on board during the cruise.

7. Station List MSM32

Tab. 4: MSM 32 Station list including ship's and internal station number.

Station No.		Date	Gear	Time	Latitude	Longitude	Water Depth	Remarks/Recovery
MERIAN	CAU	2013		[UTC]	[°N]	[°W]	[m]	
MSM32/ 589-1	MSM32-1-1	01.10.	ROS/CTD	13:53	32°54.40'	10°49.06'	4183.8	24 water samples recovered
MSM32/ 590-1	MSM32-2-1	01.10.	GC	20:14	32°54.46'	10°48.44'	4248.7	12m barrel, USBL at SL 30m, bend barrel, recovery: 159cm
MSM32/ 591-1	MSM32_ RUN#1	02.10.	TOBI	08:26	31°07.72'	10°36.13'	736.4	deep tow sidescan sonar, 495m SL max, test run
MSM32/ 592-1	MSM32-3-1	02.10.	GKG	15:06	31°08.06'	10°36.23'	719.1	USBL at SL 30m, living and dead Lophelia pertusa recovered
MSM32/ 592-2	MSM32-3-2	02.10.	ROS/CTD	16:39	31°08.06'	10°36.25'	718.4	21 water samples recovered
MSM32/ 593-1		02.10.	MB+PS	17:51	31°08.08'	10°36.27'	732.1	mapping with various course
MSM32/ 594-1	MSM32-4-1	03.10.	GKG	05:05	30°24.25'	11°29.02'	2324.5	box corer did not release, no recovery
MSM32/ 594-2	MSM32-4-2	03.10.	GC	07:39	30°24.25'	11°29.02'	2326.0	5m barrel, recovery: >500cm, overpenetrated
MSM32/ 594-3	MSM32-4-3	03.10.	GKG	09:01	32°24.25'	11°29.03'	2326.0	recovery: 38cm
MSM32/ 594-4	MSM32-4-4	03.10.	GC	11:26	30°24.25'	11°29.02'	2327.2	10m barrel, recovery: 758cm
MSM32/ 595-1	MSM32-5-1	03.10.	GC	13:59	30°26.72'	11°21.21'	2272.0	10m barrel, core catcher broken, no recovery
MSM32/ 595-2	MSM32-5-2	03.10.	GC	15:34	30°26.71'	11°21.22'	2271.7	10m barrel, recovery: 336cm
MSM32/ 596-1	MSM32-001-007	03.10.	SEISREFL	19:07	30°30.58'	11°41.30'	2224.9	several profiles, see separate list
MSM32/ 597-1		05.10.	MB+PS	10:53	29°54.89'	11°56.96'	2039.2	mapping with various course
MSM32/ 598-1	MSM32-6-1	06.10.	GC	13:50	29°14.96'	11°38.47'	1211.1	5m barrel, recovery: 485cm
MSM32/ 598-2	MSM32-7-1	06.10.	GC	15:03	29°14.69'	11°38.76'	1183.5	5m barrel, recovery: >500cm, overpenetrated
MSM32/ 598-3	MSM32-8-1	06.10.	GC	16:14	29°13.60'	11°39.96'	1125.3	5m barrel, recovery: ~580cm, overpenetrated
MSM32/ 598-4	MSM32-8-2	06.10.	GC	17:29	29°13.62'	11°39.94'	1119.6	10m barrel, recovery: 757cm
MSM32/ 599-1		06.10.	MB+PS	18:07	29°13.62'	11°39.94'	1121.2	mapping with various course
MSM32/ 600-1	MSM32_ RUN#2	07.10.	TOBI	07:17	29°06.02'	11°34.19'	3320.8	stopped due to technical problems
MSM32/ 600-2		07.10.	MB+PS	12:00	29°05.12'	11°40.42'	236.1	mapping with various course
MSM32/ 601-1	MSM32_ RUN#3	07.10.	TOBI	15:30	29°06.15'	11°35.00'	144.9	stopped due to technical problems
MSM32/ 602-1	MSM32-9-1	07.10.	GC	18:02	29°11.81'	11°35.96'	680.8	5m barrel, recovery: 488cm
MSM32/ 603-1	MSM32-10-1	07.10.	GC	18:52	29°10.12'	11°37.60'	633.0	5m barrel, recovery: 487cm
MSM32/ 604-1	MSM32-11-1	07.10.	GC	19:44	29°09.61'	11°38.62'	810.9	5m barrel, recovery: 417cm
MSM32/ 605-1	MSM32-008-013	07.10.	SEISREFL	21:11	29°03.49'	11°44.64'	412.6	several profiles, see separate list
MSM32/ 606-1		08.10.	MB+PS	19:30	29°48.96'	11°19.03'	1878.4	mapping with various course
MSM32/ 607-1	MSM32-12-1	09.10.	ROS/CTD	13:20	30°42.24'	10°59.71'	2680.0	24 water samples recovered, below ~1900m noise signal, upcast significant offset from downcast until ~800m

Station No.		Date	Gear	Time	Latitude	Longitude	Water Depth	Remarks/Recovery
MERIAN	CAU	2013		[UTC]	[°N]	[°W]	[m]	
MSM32/ 608-1		09.10.	MB+PS	15:55	30°42.33’	10°59.84’	2676.7	mapping with various course
MSM32/ 609-1	MSM32-13-1	10.10.	GC	07:20	30°35.31’	11°24.38’	2499.2	5m barrel, recovery: >500cm, overpenetrated
MSM32/ 609-2	MSM32-13-2	10.10.	GC	09:02	30°35.30’	11°24.34’	2494.6	10m barrel, recovery: 841cm
MSM32/ 610-1	MSM32-14-1	10.10.	GC	11:09	30°36.16’	11°31.32’	2450.0	10m barrel, recovery: 783cm
MSM32/ 611-1	MSM32-15-1	10.10.	GC	13:00	30°36.74’	11°36.11’	2254.5	10m barrel, recovery: 934cm
MSM32/ 612-1	MSM32_ RUN#4	10.10.	TOBI	15:11	30°28.98’	11°37.32’	2324.3	stopped due to technical problems
MSM32/ 612-2	MSM32-014	10.10.	SEISREFL	16:08	30°30.39’	11°37.08’	2298.7	stopped due to TOBI problems
MSM32/ 613-1	MSM32-015-023	10.10.	SEISREFL	20:29	30°32.86’	11°29.88’	2434.5	several profiles, see separate list
MSM32/ 614-1		12.10.	MB+PS	05:04	30°09.98’	10°42.42’	1831.1	mapping with various course
MSM32/ 615-1	MSM32-RUN#5	12.10.	TOBI	11:36	30°41.93’	10°57.62’	2647.4	towed ca. 500m above seabed with various course, stopped due to weather
MSM32/ 615-2	MSM32-024-028	12.10.	SEISREFL	12:04	30°42.53’	10°57.43’	2647.5	several profiles, see separate list
MSM32/ 616-1		15.10.	MB+PS	00:46	30°53.53’	11°35.41’	2854.3	mapping with various course
MSM32/ 617-1	MSM32-16-1	15.10.	GKG	06:12	30°45.10’	11°21.44’	2869.6	USBL at SL 30m, recovery: 39cm
MSM32/ 617-2	MSM32-16-2	15.10.	GC	08:43	30°45.16’	11°21.45’	2869.9	5m barrel, USBL at SL 30m, recovery: 171cm, barrel bounced
MSM32/ 618-1	MSM32-17-1	15.10.	GC	10:50	30°45.86’	11°23.43’	2869.7	5m barrel, recovery: 383cm
MSM32/ 619-1	MSM32-18-1	15.10.	GC	13:10	30°46.74’	11°28.25’	2841.5	10m barrel, recovery: 563cm
MSM32/ 620-1	MSM32-19-1	15.10.	GC	15:37	30°39.74’	11°25.27’	2609.4	10m barrel, recovery: 800cm
MSM32/ 621-1	MSM32-29-32	15.10.	SEISREFL	17:56	30°34.64’	11°19.10’	2396.2	several profiles, see separate list
MSM32/ 622-1	MSM32-20-1	16.10.	GC	07:35	31°04.99’	11°34.85’	3072.7	10m barrel, recovery: 559cm
MSM32/ 623-1	MSM32-21-1	16.10.	GC	11:39	31°17.01’	12°02.93’	3383.5	10m barrel, recovery: 281cm
MSM32/ 624-1		16.10.	MB+PS	13:32	31°17.13’	12°03.19’	3384.6	mapping with various course
MSM32/ 625-1	MSM32-22-1	16.10.	GC	20:44	31°56.06’	12°30.68’	3938.0	5m barrel, recovery: 320cm, hit seabed two times
MSM32/ 626-1	MSM32-33-38	16.10.	SEISREFL	22:45	31°56.24’	12°30.57’	3938.0	several profiles, see separate list
MSM32/ 627-1	MSM32-23-1	17.10.	GC	07:46	31°50.18’	12°29.08’	3888.3	5m barrel, recovery: 420cm
MSM32/ 628-1		17.10.	MB+PS	09:51	31°50.54’	12°29.20’	3891.3	mapping with various course
MSM32/ 629-1	MSM32-24-1	17.10.	GC	12:47	32°11.36’	12°32.97’	4074.3	5m barrel, no recovery
MSM32/ 630-1		17.10.	MB+PS	15:06	32°11.04’	12°30.46’	4067.9	mapping with various course
MSM32/ 631-1	MSM32-RUN#6	18.10.	TOBI	17:34	29°05.66’	11°33.38’	127.0	towed ca. 500m above seabed with various course
MSM32/ 631-2	MSM32-39	18.10.	SEISREFL	18:41	29°07.23’	11°34.64’	158.7	several profile, see separate list
MSM32/ 632-1		19.10.	MB+PS	18:14	29°48.10’	12°12.59’	1943.8	mapping with various course
MSM32/	MSM32-	19.10.	SEISREFL	20:31	29°32.58’	12°05.33’	1775.4	several profiles, see separate list

Station No.		Date	Gear	Time	Latitude	Longitude	Water Depth	Remarks/Recovery
MERIAN	CAU	2013		[UTC]	[°N]	[°W]	[m]	
632-2	40-45’							
MSM32/ 633-1	MSM32- 25-1	20.10.	GC	07:13	29°47.13’	12°07.74’	1938.5	10m barrel, recovery: 673cm, may have bounced
MSM32/ 634-1	MSM32- 26-1	20.10.	GC	08:40	29°47.75’	12°08.30’	1953.1	10m barrel, recovery: 890cm, may have bounced
MSM32/ 635-1	MSM32- 27-1	20.10.	GC	10:58	29°44.67’	12°05.64’	1937.7	10m barrel, recovery: 669cm
MSM32/ 636-1		20.10.	MB+PS	12:16	29°45.61’	12°05.77’	1942.8	mapping with various course
MSM32/ 637-1	MSM32- 28-1	20.10.	GC	15:19	30°04.35’	11°47.69’	2175.8	10m barrel, recovery: 806cm
MSM32/ 638-1	MSM32- 29-1	20.10.	GC	17:24	30°02.63’	11°46.26’	2193.4	10m barrel, recovery: 794cm
MSM32/ 639-1		20.10.	MB+PS	18:46	30°02.56’	11°46.12’	2182.8	mapping with various course
MSM32/ 639-2	MSM32- 46-50	20.10.	SEISREFL	23:34	29°26.43’	11°39.99’	1540.3	several profiles, see separate list
MSM32/ 640-1	MSM32- 30-1	21.10.	GC	07:11	29°18.20’	11°45.95’	1458.9	10m barrel, recovery: 151cm
MSM32/ 641-1		21.10.	MB+PS	13:04	29°12.24’	10°48.94’	95.8	mapping with various course
MSM32/ 641-2	MSM32- 51	22.10.	SEISREFL	08:56	30°12.79’	09°48.18’	98.7	several profiles, see separate list
MSM32/ 642-1	MSM32- 31-1	23.10.	GKG	07:16	29°55.49’	10°00.94’	137.7	recovery: 18cm
MSM32/ 642-2	MSM32- 31-2	23.10.	GC	07:42	29°55.49’	10°00.95’	136.4	5m barrel, no recovery
MSM32/ 643-1		23.10.	MB+PS	08:16	29°56.04’	10°00.15’	126.7	mapping with various course
MSM32/ 644-1	MSM32- 32-1	23.10.	GKG	08:57	29°54.68’	10°01.50’	149.3	recovery: 25cm
MSM32/ 645-1	MSM32- 33-1	23.10.	GKG	09:35	29°53.80’	10°00.20’	122.9	no recovery, corer did not close
MSM32/ 645-2	MSM32- 33-2	23.10.	GKG	10:01	29°53.80’	10°00.20’	123.8	recovery: 20.5cm
MSM32/ 645-3	MSM32- 33-3	23.10.	GC	10:20	29°53.80’	10°00.21’	124.3	5m barrel, liner empty
MSM32/ 646-1	MSM32- 34-1	23.10.	GKG	11:12	29°52.76’	09°58.09’	109.4	recovery: 21cm
MSM32/ 647-1		23.10.	MB+PS	11:27	29°52.76’	09°58.09’	108.3	mapping with various course
MSM32/ 648-1	MSM32- 35-1	23.10.	GKG	12:33	29°56.88’	10°07.16’	653.2	SVP beacon at SL 30m, recovery: 41cm
MSM32/ 648-2	MSM32- 35-2	23.10.	GC	13:16	29°56.88’	10°07.16’	627.0	5m barrel, recovery: 100cm, bend barrel
MSM32/ 649-1		23.10.	MB+PS	13:54	29°57.46’	10°07.77’	477.5	mapping upper canyon with various course
MSM32/ 650-1	MSM32- 36-1	23.10.	GKG	20:43	30°29.49’	11°10.28’	2619.1	USBL at SL 30m, recovery: 25cm
MSM32/ 651-1	MSM32- 37-1	23.10.	GC	23:06	30°29.66’	11°10.03’	2600.8	10m barrel, recovery: 201cm
MSM32/ 652-1		24.10.	MB+PS	02:40	30°48.33’	10°51.56’	2065.9	mapping with various course
MSM32/ 653-1	MSM32- 38-1	24.10.	GKG	13:14	30°09.34’	09°53.55’	133.5	recovery: 27.5cm
MSM32/ 654-1	MSM32- 39-1	24.10.	GKG	14:15	30°15.52’	09°52.37’	123.8	recovery: 27cm
MSM32/ 655-1	MSM32- 40-1	24.10.	GKG	14:51	30°17.76’	09°52.12’	114.9	box corer empty
MSM32/ 655-2	MSM32- 40-2	24.10.	GKG	15:04	30°17.76’	09°52.12’	114.8	box corer empty
MSM32/	MSM32-	24.10.	BP	15:29	30°17.76’	09°52.12’	115.6	recovery: ~5cm

Station No.		Date	Gear	Time	Latitude	Longitude	Water Depth	Remarks/Recovery
MERIAN	CAU	2013		[UTC]	[°N]	[°W]	[m]	
655-3	40-3							
MSM32/ 656-1	MSM32- 41-1	24.10.	CTD/ROS	16:09	30°18.17’	09°47.44’	96.9	no samples taken
MSM32/ 656-2	MSM32- 41-2	24.10.	GKG	16:27	30°18.17’	09°47.45’	93.6	recovery: 40cm
MSM32/ 656-3	MSM32- 41-3	24.10.	GC	16:41	30°18.17’	09°47.45’	97.0	5m barrel, recovery: 150cm
MSM32/ 657-1	MSM32- 42-1	24.10.	GKG	16:56	30°26.00’	09°42.73’	46.2	recovery: 43cm
MSM32/ 657-2	MSM32- 42-2	24.10.	GC	18:03	30°26.00’	09°42.72’	46.7	5m barrel, recovery: 106cm
MSM32/ 658-1	MSM32- 43-1	24.10.	GKG	18:50	30°24.78’	09°49.52’	96.9	recovery: 39cm
MSM32/ 658-2	MSM32- 43-2	24.10.	GC	19:11	30°24.79’	09°49.52’	96.0	5m barrel, recovery: 143cm
MSM32/ 659-1	MSM32- 44-1	24.10.	GKG	21:43	30°48.72’	10°00.87’	93.4	recovery: 42cm
MSM32/ 660-1		24.10.	MB+PS	21:52	30°48.72’	10°00.87’	93.7	mapping with various course
MSM32/ 661-1	MSM32- 45-1	25.10.	GKG	07:55	31°18.94’	10°40.29’	701.4	USBL at SL 30m, recovery: 21cm
MSM32/ 662-1	MSM32- 46-1	25.10.	GKG	09:32	31°25.09’	10°40.06’	801.7	USBL at SL 17m, recovery: 35cm
MSM32/ 663-1	MSM32- 47-1	25.10.	GKG	11:00	31°21.02’	10°44.79’	834.9	USBL at SL 20m, recovery: 70cm
MSM32/ 664-1	MSM32- 48-1	25.10.	GKG	12:55	31°12.47’	10°42.85’	863.8	USBL at SL 20m, recovery: 24cm
MSM32/ 665-1	MSM32- 49-1	25.10.	GKG	14:19	31°12.74’	10°37.53’	676.7	USBL at SL 14m, no recovery, box corer turned to side, wire tangled around framework
MSM32/ 665-2	MSM32- 49-2	25.10.	GKG	15:08	31°12.74’	10°37.54’	678.2	USBL at SL 14m, recovery: 45cm
MSM32/ 666-1	MSM32- 50-1	25.10.	GKG	16:20	31°09.79’	10°38.23’	782.3	USBL at SL 20m, no recovery
MSM32/ 666-2	MSM32- 50-2	25.10.	GKG	17:18	31°09.78’	10°38.25’	788.2	USBL at SL 17m, recovery: 27.5cm
MSM32/ 667-1	MSM32- 51-1	25.10.	ROS/CTD	18:37	31°12.74’	10°37.53’	685.4	JoJo-CTD: count 1 14 water samples recovered, data recording did not work, to be repeated
MSM32/ 667-2	MSM32- 51-2	25.10.	ROS/CTD	19:52	31°12.74’	10°37.53’	683.5	JoJo-CTD: count 2 14 water samples recovered
MSM32/ 667-3	MSM32- 51-3	25.10.	ROS/CTD	21:38	31°12.75’	10°37.53’	699.0	JoJo-CTD: count 3 2 bottom water samples: 665m
MSM32/ 667-4	MSM32- 51-4	25.10.	ROS/CTD	22:25	31°12.75’	10°37.53’	681.8	JoJo-CTD: count 4 2 bottom water samples: 670m
MSM32/ 667-5	MSM32- 51-5	25.10.	ROS/CTD	23:17	31°12.75’	10°37.53’	681.1	JoJo-CTD: count 5 2 bottom water samples: 672m
MSM32/ 667-6	MSM32- 51-6	26.10.	ROS/CTD	00:05	31°12.75’	10°37.53’	679.3	JoJo-CTD: count 6 2 bottom water samples: 675m
MSM32/ 667-7	MSM32- 51-7	26.10.	ROS/CTD	00:46	31°12.75’	10°37.53’	678.0	JoJo-CTD: count 7 2 bottom water samples: 676m
MSM32/ 667-8	MSM32- 51-8	26.10.	ROS/CTD	01:28	31°12.74’	10°37.53’	676.8	JoJo-CTD: count 8 2 bottom water samples: 676m
MSM32/ 667-9	MSM32- 51-9	26.10.	ROS/CTD	02:07	31°12.74’	10°37.53’	678.2	JoJo-CTD: count 9 2 bottom water samples: 676m
MSM32/ 667-10	MSM32- 51-10	26.10.	ROS/CTD	02:49	31°12.75’	10°37.53’	684.5	JoJo-CTD: count 10 2 bottom water samples: 677m
MSM32/ 667-11	MSM32- 51-11	26.10.	ROS/CTD	04:32	31°12.75’	10°37.54’	689.7	JoJo-CTD: count 11 2 bottom water samples: 677m
MSM32/ 667-12	MSM32- 51-12	26.10.	ROS/CTD	05:21	31°12.75’	10°37.54’	687.7	JoJo-CTD: count 12 2 bottom water samples: 677m

Station No.		Date	Gear	Time	Latitude	Longitude	Water Depth	Remarks/Recovery
MERIAN	CAU	2013		[UTC]	[°N]	[°W]	[m]	
MSM32/ 667-13	MSM32-51-13	26.10.	ROS/CTD	06:05	31°12.75’	10°37.53’	682.8	JoJo-CTD: count 13 2 bottom water samples: 675m
MSM32/ 667-14	MSM32-51-14	26.10.	ROS/CTD	06:49	31°12.75’	10°37.53’	681.1	JoJo-CTD: count 14 2 bottom water samples: 673m
MSM32/ 667-15	MSM32-51-15	26.10.	ROS/CTD	07:45	31°12.75’	10°37.53’	683.8	JoJo-CTD: count 15 8 water samples recovered
MSM32/ 668-1	MSM32-52-1	26.10.	ROS/CTD	09:39	31°12.73’	10°34.49’	623.8	8 water samples recovered
MSM32/ 669-1	MSM32-50-3	26.10.	ROS/CTD	11:02	31°09.78’	10°38.24’	785.2	8 water samples recovered
MSM32/ 670-1	MSM32-48-2	26.10.	ROS/CTD	12:38	31°12.47’	10°42.85’	934.4	8 water samples recovered
MSM32/ 671-1	MSM32-45-2	26.10.	ROS/CTD	14:37	31°18.95’	10°40.32’	702.5	8 water samples recovered
MSM32/ 672-1	MSM32-46-2	26.10.	ROS/CTD	16:17	31°25.09’	10°40.06’	793.9	8 water samples recovered
MSM32/ 673-1	MSM32-47-2	26.10.	ROS/CTD	17:55	31°21.02’	10°44.79’	835.3	8 water samples recovered
MSM32/ 674-1	MSM32-52-54	26.10.	SEISREFL	19:27	31°20.58’	10°49.77’	994.5	several profiles, see separate list
MSM32/ 675-1	MSM32-53-1	27.10.	GC	08:13	30°30.70’	10°50.26’	2099.0	10m barrel, recovery: 802cm
MSM32/ 676-1		27.10.	MB+PS	10:56	30°46.73’	10°58.79’	2156.5	mapping with various course
MSM32/ 677-1	MSM32-54-1	27.10.	GC	16:22	31°16.03’	10°50.56’	3185.0	10m barrel, recovery: 531cm
MSM32/ 678-1		27.10.	MB+PS	19:04	31°24.50’	11°58.98’	2806.1	mapping with various course
MSM32/ 679-1	MSM32-55-1	27.10.	GC	22:03	31°42.69’	12°23.99’	3804.5	5m barrel, recovery: 187cm
MSM32/ 680-1	MSM32-56-1	28.10.	GC	01:12	31°53.43’	12°30.18’	3910.7	5m barrel, recovery: 238cm
MSM32/ 681-1		28.10.	MB+PS	03:08	31°53.46’	12°30.00’	3914.7	mapping with various course
MSM32/ 682-1	MSM32-55-56	28.10.	SEISREFL	08:45	32°44.51’	12°51.00’	3527.4	several profiles, see separate list
MSM32/ 683-1	MSM32-57-1	28.10.	GC	18:36	31°55.14’	12°30.49’	3929.4	5m barrel, recovery: 157cm

Tab. 5: List of seismic profiles.

Prof-Nr.	Date 2013	Time Start UTC	Time End UTC	Latitude Start xx° xx.x‘	Longitude Start xx° xx.x‘	Latitude End xx° xx.x‘	Longitude End xx° xx.x‘	Geometrics FFN Start FFN Start	Geometrics FFN End FFN End
001	03./04.10.	20:41	13:45	30° 28.72'	11° 44.13'	29° 17.79'	10° 49.69'	**400**	**10615**
002	04.10.	13:45	15:58	29° 17.79'	10° 49.69'	29° 13.54'	11° 01.29'	**10616**	**11944**
003	04.10.	15:58	17:14	29° 13.54'	11° 01.29'	29° 18.87'	11° 04.76'	**11945**	**12698**
004	04./05.10.	17:14	00:32	29° 18.87'	11° 04.76'	29° 34.86'	11° 39.05’	**12699**	**17077**
005	05.10.	00:32	06:56	29° 34.86'	11° 39.05‘	29° 57.43'	11° 53.57'	**17078**	**20913**
006	05.10.	06:56	08:32	29° 57.43'	11° 53.57'‘	29° 53.92'	12° 01.82'	**20914**	**21882**
007	05.10.	08:32	09:29	29° 53.92'	12° 01.82'	29° 49.29'	12° 01.67'	**21883**	**22438**
008	07./08.10.	21:57	00:50	29° 05.85'	11° 44.41'	29° 14.27'	11° 14.28'	**23122**	**24861**
009	08.10.	00:53	01:53	29° 14.38'‘	11° 30.82'	29° 16.56’	11° 25.81’	**24862**	**25485**
010	08.10.	01:53	02:41	29° 16.56‘	11° 25.81‘	29° 19.45’	11° 28.10’	**25486**	**25963**
011	08.10.	02:41	06:45	29° 19.45‘	11° 28.10‘	29° 09.84’	11° 46.03’	**25964**	**28409**
012	08.10.	06:45	08:14	29° 09.84‘	11° 46.03‘	29° 15.07’	11° 50.23’	**28410**	**29298**

Prof-Nr.	Date 2013	Time Start UTC	Time End UTC	Latitude Start xx° xx.x‘	Longitude Start xx° xx.x‘	Latitude End xx° xx.x‘	Longitude End xx° xx.x‘	Geometrics FFN Start FFN Start	Geometrics FFN End FFN End
013	08.10.	08:14	18:17	29° 15.07’	11° 50.23’	29° 48.39’	11° 11.52’	**29299**	**35322**
014	10.10.	16:28	18:50	30° 31.05’	11° 26.75’	30° 35.93’	11° 33.89’	**36010**	**37127**
015	10./11.10.	20:48	01:10	30° 33.54’	11° 29.71’	30° 51.80’	11° 20.42’	**38000**	**40242**
016	11.10.	01:10	01:42	30° 51.80’	11° 20.42’	30° 53.36’	11° 22.83’	**40243**	**40513**
017	11.10.	01:42	5:48	30° 53.36’	11° 22.83’	30° 37.80’	11° 34.96’	**40514**	**42622**
018	11.10.	5:48	08:54	30° 37.80’	11° 34.96’	30° 34.58’	11° 18.75’	**42623**	**44221**
019	11.10.	08:54	12:48	30° 34.58’	11° 18.75’	30° 34.86’	10° 56.86’	**44222**	**46223**
020	11.10.	12:48	16:00	30° 34.86’	10° 56.86’	30° 50.84’	10° 55.08’	**46224**	**47899**
021	11.10.	16:00	18:50	30° 50.97’	10° 54.80’	30° 47.94’	10° 39.41’	**48000**	**49638**
022	11.10.	18:50	23:58	30° 47.94’	10° 39.41’	30° 27.28’	10° 22.07’	**49639**	**52717**
023	11./12.10.	23:58	03:45	30° 27.28’	10° 22.07’	30° 13.92’	10° 38.77’	**52718**	**55074**
024	12.10.	12:48	21:45	30° 42.87’	10° 59.00’	30° 46.36’	11° 24.52’	**56015**	**60620**
025	12./13.10.	21:45	01:03	30° 46.36’	11° 24.52’	30° 52.99’	11° 30.54’	**60621**	**62312**
026	13.10.	01:03	06:02	30° 52.99’	11° 30.54’	31° 04.79’	11° 35.02’	**62313**	**64868**
027	13.10.	06:02	14:18	31° 04.79’	11° 35.02’	31° 15.95’	11° 54.07’	**64869**	**69118**
028	13.10.	14:18	21:17	31° 15.95’	11° 54.07’	31° 20.397’	12° 13.45’	**69119**	**72714**
029	15.10.	18:34	22:27	30° 37.09’	11° 18.68’	30° 45.98’	11° 35.82’	**73180**	**75179**
030	15./16.10	22:27	02:03	30° 45.98’	11° 35.82’	30° 57.88’	11° 25.01’	**75180**	**77023**
031	16.10.	02:03	02:31	30° 57.88’	11° 25.01’	30° 59.79’	11° 26.44’	**77024**	**77262**
032	16.10.	02:31	05:46	30° 59.79’	11° 26.44’	30° 55.92’	11° 43.04’	**77263**	**78931**
033	16./17.10	23:47	00:59	31° 56.10’	12° 31.55’	31° 50.37’	12° 29.80’	**79274**	**79810**
034	17.10.	00:59	01:56	31° 50.37’	12° 29.80’	31° 49.21’	12° 24.41’	**79811**	**80237**
035	17.10.	01:56	02:03	31° 49.21’	12° 24.41’	31° 48.57’	12° 24.32’	**80238**	**80295**
036	17.10.	02:03	03:31	31° 48.57’	12° 24.32’	31°47.09’	12° 32.62’	**80296**	**80951**
037	17.10.	03:31	04:53	31° 47.09’	12° 32.62’	31° 53.45’	12° 35.04’	**80952**	**81570**
038	17.10.	04:53	06:34	31° 53.45’	12° 35.04’	31° 55.03’	12° 26.17’	**81571**	**82325**
039	18./19.10.	18:46	12:53	29° 07.40’	11° 34.77’	29° 44.26’	12° 05.30’	**83000**	**93854**
040	19.10.	20:44	21:41	29° 32.88’	12° 04.81’	29° 35.76’	12° 00.99’	**94040**	**94718**
041	19.10.	21:41	22:21	29° 35.76’	12° 00.99’	29° 34.71’	11° 57.56’	**94719**	**95198**
042	19./20.10.	22:21	01:29	29° 34.71’	11° 57.56’	29° 36.99’	11° 40.04’	**95199**	**97455**
043	20.10.	01:29	01:38	29° 36.99’	11° 40.04’	29° 37.67’	11° 40.25’	**97456**	**97560**
044	20.10.	01:38	03:58	29° 37.67’	11° 40.25’	29° 40.91’	11° 53.04’	**97561**	**99245**
045	20.10.	03:58	06:16	29° 40.91’	11° 53.04’	29° 49.45’	12° 01.81’	**99246**	**100803**
046	20./21.10.	23:49	00:09	29° 25.63’	11° 40.40’	29° 24.17’	11° 41.02’	**100100**	**101280**
047	21.10.	00:09	02:59	29° 24.17’	11° 41.02’	29° 11.13’	11° 34.57’	**101281**	**103319**
048	21.10.	02:59	3:35	29° 10.90’	11° 34.74’	29° 09.16’	11° 37.10’	**103320**	**103757**
049	21.10.	3:35	4:42	29° 09.16’	11° 37.10’	29° 13.45’	11° 40.93’	**103758**	**104562**
050	21.10.	4:42	6:20	29° 13.45’	11° 40.93’	29° 17.29’	11° 49.28’	**104563**	**105736**
051	22.10.	09:04	14:17	30° 12.27’	09° 48.30’	29° 48.99’	10° 00.89’	**106000**	**110677**
052	26.10.	20:03	23:05	31° 22.12’	10° 50.75’	31° 18.91’	10° 33.28’	**111241**	**113437**
053	26./27.10.	23:05	0:04	31° 18.91’	10° 33.28’	31° 14.20’	10° 31.92’	**113438**	**114140**
054	27.10.	00:04	04:03	31° 14.20’	10° 31.92’	31° 09.28’	10° 52.75’	**114141**	**116990**
055	28.10.	09:03	13:14	32° 45.06’	12° 50.06’	32° 27.47’	12° 42.58’	**117068**	**119110**
056	28.10.	13:14	15:11	32° 27.47’	12° 42.58’	32°27.67’	12°31.73’	**119111**	**120096**

8. Data and Sample Storage and Availability

All meta-data of the cruise were made available immediately after the cruise via the Kiel data portal for marine science (https://portal.geomar.de/metadata/leg/show/319158).

The seismic, bathymetric and hydro-acoustic raw data as well as processed seismic data are archived on a dedicated server at Kiel University. The acoustic data will be submitted to a public data base as soon as such a data base for long-term archival will be available and standards for archiving have been defined. The moratorium for exclusive use by MSM32 scientists is set to three years until November 1st, 2016. Thereafter the data will be available for other scientists upon request. Contact person is cruise leader Sebastian Krastel (skrastel@geophysik.uni-kiel.de).

All cores are stored and archived in the Kiel core repository. The MSM32 scientific party has a three-year moratorium time until November 1st, 2016, for exclusive analytical work before the cores will be available for sampling by other scientists upon reasonable statement. All data measured at the cores during the cruise and post cruise will be included in the PANGAEA data base in Bremerhaven, which will then provide long-term archival and access to the data within WDC-MARE.

9. Acknowledgements

The scientific party of Cruise MSM32 gratefully acknowledges the very friendly and most effective cooperation with Captain Schmidt and his crew. Their perfect technical assistance and great flexibility made this cruise a scientific success. We also appreciate the valuable support by the Leitstelle Deutsche Forschungsschiffe at the University of Hamburg. This expedition was funded by the Deutsche Forschungsgemeinschaft (DFG) and the Bundesministerium für Bildung und Forschung (BMBF).

10. References

Bondevik, S., Lovholt, F., Harbitz, C.B., Mangerud, J., Dawson, A.G., Svendsen, J.I. (2005) The Storegga Slide tsunami - comparing field observations with numerical simulations. Marine Petroleum Geology, 22, 195-208.

Camerlenghi, A., Urgeles, R., Ercilla, G., Brückmann, W. (2007) Scientific Ocean Drilling Behind the Assessment of Geo-Hazards from Submarine Slides. Scientific Drilling, 4, 45-47.

Dullo, W.-C., Flögel, S., Rüggeberg, A. (2008). Cold-water coral growth in relation to the hydrography of the Celtic and Nordic European continental margin, Mar Ecol Prog Ser, 371, 165-176.

Felwellen, C., Millard, N., Rouse, I. (1993) TOBI, a vehicle for deep ocean survey. Electronics & Communication Egeneering Journal, April 1993, 85-93.

Galy, V., France-Lanord, C., Beyssac, O., Faure, P., Kudrass, H., Palhol, F., 2007. Efficient organic carbon burial in the Bengal fan sustained by the Himalayan erosional system. Nature, 450, 407-411.

Graßhoff, K. (1983) Determination of oxygen. In: Grasshoff, K., Ehrhardt. M., Kremling, K. (Eds.) Methods of seawater analysis. Verlag Chemie Weinheim, New York, pp. 61-72.

Mittelstaedt, E. (1991). The ocean boundary along the northwest African coast: Circulation and oceanographic properties at the sea surface, Prog. Oceanography, 26, 307-355.

Morigi, C., Jorissen, F.J., Gervais, S., Borsetti, A.M. (2001). Benthic foraminiferal faunas in surface sediments off NW Africa: Relationship with organic flux to the ocean floor. Journal of Foraminiferal research, 31, 350-368.

Mosher, D.C., Lee, H., Urgeles, R., Shipp, R.C., Moscardelli, L. (2010) Submarine Mass Movements and Their Consequences. Advances in Natural and Technological Hazards, 28, Springer, 786 pp.

Sarnthein, M., Thiede, J., Pflaumann, U., Erlenkeuser, H., Fütterer, D.K., Koopmann, B., Lange, H., Seibold, E. (1982) Atmospheric and oceanic circulation patterns off Northwest Africa during the past 25 million years. In: von-Rad, U. Hinz, K., Sarnthein, M., Seibold, E. (eds.), Geology of the Northwest African continental margin: Springer-Verlag, Berlin, pp. 545-604.

Siddall, M., Rohling, E.J., Almogi-Labin, A., Hemleben, Ch., Meischner, D., Schmelzer, I., Smeed, D.A. (2003) Sea-level fluctuations during the last glacial cycle. Nature, 423, 853-858.

Tappin, D.R., Watts, P., McMurtry, G.M., Lafoy, Y., Matsumoto, T. (2001) The Sissano, Papua New Guinea tsunami of July 1998 – offshore evidence on the source mechanism. Marine Geology, 175, 1-23.

Wynn, R.B., Talling, P.J., Masson, D.G., Stevenson, C.J., Cronin, B.T., Le Bas., T.P. (2010) Investigating the timing, processes and deposits of one the World's largest submarine gravity flows: the 'Bed 5 event' off northwest Africa. In Mosher, D.C., Moscardelli, L., Shipp, C., Chaytor, J.D., Baxter, D.P., Lee, H.J. and Urgeles, R. (eds) Submarine mass movements and their consequences: Advances in Natural and Technological Hazards Research, 28, Springer, 463-474.